Mon. Not. R. Astron. Soc. **338,** 687–710 (2003)

Heavy elements in Galactic and Magellanic Cloud H II regions: recombination-line versus forbidden-line abundances

Yiannis G. Tsamis,[1] M. J. Barlow,[1]★ X.-W. Liu,[1] I. J. Danziger[2] and P. J. Storey[1]

[1]*Department of Physics and Astronomy, University College London, Gower Street, London WC1E 6BT*
[2]*Osservatorio Astronomico di Trieste, Via G. B. Tiepolo 11, I-34131 Trieste, Italy*

Accepted 2002 September 18. Received 2002 September 13; in original form 2002 July 22

ABSTRACT

We have obtained deep optical, long-slit spectrophotometry of the Galactic H II regions M 17, NGC 3576 and of the Magellanic Cloud H II regions 30 Doradus, LMC N11B and SMC N66, recording the optical recombination lines (ORLs) of C II, N II and O II. A spatial analysis of 30 Doradus is performed, revealing that the forbidden-line [O III] electron temperature is remarkably constant across the nebula. The forbidden-line O^{2+}/H^+ abundance mapped by the [O III] λ4959 collisionally excited line (CEL) is shown to be consistently lower than the recombination-line abundance mapped by the O II V1 multiplet at 4650 Å. In addition, the spatial profile of the C^{2+}/O^{2+} ratio derived purely from recombination lines is presented for the first time for an extragalactic nebula. Temperature-insensitive ORL C^{2+}/O^{2+} and N^{2+}/O^{2+} ratios are obtained for all nebulae except SMC N66. The ORL C^{2+}/O^{2+} ratios show remarkable agreement within each galactic system, while also being in agreement with the corresponding CEL ratios. The disagreement found between the ORL and CEL N^{2+}/O^{2+} ratios for M 17 and NGC 3576 can be attributed to the N II V3 and V5 ORLs that were used being affected by fluorescent excitation effects.

For all five nebulae, the O^{2+}/H^+ abundance derived from multiple O II ORLs is found to be higher than the corresponding value derived from the strong [O III] λλ4959, 5007 CELs, by factors of 1.8 to 2.7 for four of the nebulae. The LMC N11B nebula exhibits a more extreme discrepancy factor for the O^{2+} ion, ∼5. Thus, these H II regions exhibit ORL/CEL abundance discrepancy factors that are similar to those previously encountered amongst planetary nebulae.

Our optical CEL O^{2+}/H^+ abundances agree to within 20–30 per cent with published O^{2+}/H^+ abundances that have been obtained from observations of infrared fine-structure lines. Since the low excitation energies of the latter make them insensitive to variations about typical nebular temperatures, fluctuations in temperature are ruled out as the cause of the observed ORL/CEL O^{2+} abundance discrepancies. We present evidence that the observed O II ORLs from these H II regions originate from gas of very similar density (<3500 cm^{-3}) to that emitting the observed heavy-element optical and infrared CELs, ruling out models that employ high-density ionized inclusions in order to explain the abundance discrepancy. We consider a scenario whereby much of the heavy-element ORL emission originates from cold ($\leqslant 500$ K) metal-rich ionized regions. These might constitute haloes that are being evaporated from much denser neutral cores. The origin of these metal-rich inclusions is not clear – they may have been ejected into the nebula by evolved, massive Of and Wolf–Rayet stars, although the agreement found between heavy-element ion ratios derived from ORLs with the ratios derived from CELs provides no evidence for nuclear-processed material in the ORL-emitting regions.

Key words: stars: individual: R139 – stars: individual: R140 – stars: individual: P3157 – ISM: abundances – H II regions.

★E-mail: mjb@star.ucl.ac.uk

1 INTRODUCTION

In recent years, deep spectroscopic studies, coupled with new theoretical results in atomic physics, have cast new light on a well-established field of modern astrophysics: the study of elemental abundances in H II regions (ionized gas clouds marking the birthplaces of stars within the galaxy and in external galaxies) and planetary nebulae (PNe; ionized ejected envelopes of evolved low- to intermediate-mass stars). On the one hand, an accurate knowledge of abundances in galactic and extragalactic H II regions is of paramount importance for constraining galactic chemical evolution models (e.g. Shields 2002). On the other hand, abundance studies of PNe provide useful constraints on nucleosynthetic theories and our understanding of the late stages of stellar evolution (Kingsburgh & Barlow 1994; Henry, Kwitter & Bates 2000). Nebular abundances of heavy elements such as C, N, O and Ne, relative to H, have traditionally been derived from observations of strong, and thus easy to measure, collisionally-excited ionic lines (CELs); e.g. C III] λλ1906, 1909, [N II] λλ6548, 6584, [O III] λλ4959, 5007 and [Ne III] λλ3869, 3967. However, the analysis of observations of weak heavy-element optical recombination lines (ORLs) from PNe, including publications by Peimbert, Storey & Torres-Peimbert (1993), Liu et al. (1995a, 2000, 2001b), Luo, Liu & Barlow (2001), Garnett & Dinerstein (2001), and the recent work of Tsamis et al. (2003a, for observations and CEL analysis; 2003b for ORL analysis), have yielded CNONe abundances for PNe that are systematically higher than those derived using the standard CEL method. The most promising explanation for these results, at least for PNe, posits the existence within nebulae of a hitherto unknown, low-temperature component enhanced in heavy elements and emitting mostly in ORLs, intermingled with a hot component of more normal composition from which the CEL emission originates (Liu et al. 2000; Liu 2002a,b; Péquignot et al. 2002a,b). The exact nature and origin of the putative ORL-emitting component is currently a matter of intense debate.

The ORL results for PNe become a matter of concern for nebular abundance studies, all the more so because nebular CEL abundances have been long plagued by lingering doubts about their reliability, arising from their exponential sensitivity to the adopted nebular electron temperature and their dependence on the adopted nebular electron density (for lines of low critical density, N_{cr}; Rubin 1989). On the other hand, elemental abundances relative to hydrogen derived from ratios of ORLs [e.g. from the I(C II λ4267)/I(Hβ) intensity ratio for the derivation of C^{2+}/H^+, as opposed to using the CEL/ORL I(λ1908)/I(Hβ) ratio] are nearly independent of both the adopted temperature and density; this means that abundance determinations employing ORLs should be more accurate than those using CELs, because in real nebulae much of the emission of CELs can be biased towards regions of high electron temperature, as well as towards regions having electron densities less than the critical density of the CEL. As a result, ORL abundance studies of ionized nebulae are now coming to the fore, thanks also to rapid progress in detector technology.

To date, deep abundance studies of PNe (summarized by Liu 2002b) have yielded ORL abundances for C, N, O and Ne which, for the majority (90–95 per cent) of nebulae, are typically a factor of 2–3 larger than those obtained from ultraviolet (UV), optical or infrared (IR) CELs. For the remaining 5–10 per cent of PNe, even larger discrepancy factors (5–80) are found between the heavy-element abundances derived from ORLs and CELs. The situation for H II regions is less clear thus far than for PNe, mainly on account of the small number of H II regions so far observed specifically for the purpose of detecting heavy-element ORLs and deriving abundances from them. Peimbert et al. (1993) found ORL O^{2+}/H^+ abundances for M 42 and M 17 that were a factor of 2 larger than those found from the [O III] optical CELs, while Esteban et al. (1998, 1999) found ORL O^{2+} abundances that were larger than the CEL values by a factor of 1.5 for M 42 and a factor of 2 for M 8. Clearly, if H II regions are generally found to yield heavy-element abundances from ORLs that exceed those from CELs by similar factors to those summarized above for PNe and for M 8, M 17 and M 42, then this could have serious implications for our understanding of the chemical evolution of galaxies, which to date has relied to a large extent on CEL abundance analyses of H II regions located in our own and other galaxies. In this paper, we aim to increase the number of H II regions with ORL abundance analyses, by presenting deep, medium-resolution, long-slit optical spectrophotometry of the bright Galactic H II regions M 17 and NGC 3576, and the Magellanic Cloud H II regions 30 Doradus, LMC N11B and SMC N66. These nebulae were selected to be of relatively high excitation for H II regions, with O^{2+} being the dominant ion stage of oxygen. In Section 2 we describe our optical spectroscopic observations and present a thorough list of emission line fluxes and dereddened intensities. In Section 3 we describe the extinction corrections and the plasma temperature and density analysis. In Section 4 we present an abundance analysis using optical collisionally excited lines. In Section 5 we present an abundance study using optical recombination lines, discussing the relative intensities of O II ORLs and complications arising from the presence of bright dust-scattered starlight within the nebulae. In Section 6 high-resolution long-slit spectra of 30 Doradus are used to map the electron temperature and density, and the ionic abundances across the nebular surface. Finally, we discuss the implications of the results from this extensive study in Section 7 and state our conclusions in Section 8.

2 OBSERVATIONS AND DATA REDUCTION

The observational data set consists of long-slit spectra obtained during runs at the European Southern Observatory (ESO) using the 1.52-m telescope and the 3.5-m New Technology Telescope (NTT). Additional long-slit spectroscopy for one target was performed at the 3.9-m Anglo-Australian Telescope (AAT). The journal of observations is presented in Table 1.

The Galactic H II regions M 17 and NGC 3576 were observed at the ESO with the B&C spectrograph on the 1.52-m telescope. The detector was a Loral 2048 × 2048, 15 × 15 μm^2 CCD in 1996 July and in 1997 February. A 2-arcsec wide, 3.5-arcmin long slit was employed. The CCDs were binned by a factor of 2 along the slit direction, in order to reduce the readout noise. The spatial sampling was 1.63 arcsec per pixel projected on the sky. Two wavelength regions of M 17 were observed in 1996 July: a 2400 lines mm^{-1} holographic grating was used in first order to cover the 3995–4978 Å range at a spectral resolution of 1.5 Å (FWHM); a second grating in first order, along with a WG345 order sorting filter, was used to cover the 3535–7400 Å range at a resolution of 4.5 Å. The shortest integration time was chosen so as to ensure that strong emission lines such as Hα and [O III] λλ4959, 5007 would not be saturated. NGC 3576 was observed in 1997 February, in the 3995–4978 Å range only, at a resolution of 1.5 Å. Additional spectra of NGC 3576 were taken at the AAT with the RGO spectrograph and a TEK 1024 × 1024, 24 × 24 μm^2 CCD. A 1200 lines mm^{-1} grating was used in second order with two settings to cover the 3509–3908 and 3908–4305 Å ranges, at a resolution of 1 Å, while a 250 lines mm^{-1} grating was used to cover the 3655–7360 Å range in first

Table 1. Journal of observations.

H II region	Date (UT)	λ-range (Å)	FWHM (Å)	PA (deg)	RA (2000)	DEC (2000)	Exp. (s)
			ESO 1.52-m				
M 17	96/7/07	3995–4978	1.5	−21	18 20 40.0	−16 09 29	3 × 1200
M 17	96/7/13	3535–7400	4.5	−21	”	”	60, 300, 600
NGC 3576	97/2/11	3995–4978	1.5	−50	11 11 56.9	−61 17 25	6 × 1800
			AAT 3.9-m				
NGC 3576	95/2/08	3509–3908	1	−50	11 12 00.5	−61 18 24	300, 1800
NGC 3576	”	3908–4305	1	−50	”	”	2 × 1800
NGC 3576	”	3635–7360	8.5	−50	”	”	120, 300, 600
			NTT 3.5-m				
30 Doradus	95/12/15	3635–4145	2	76	05 38 45.6	−69 05 24	3 × 1200
30 Doradus	”	4060–4520	2	76	”	”	3 × 1200
30 Doradus	”	4515–4975	2	76	”	”	300, 4 × 1200
30 Doradus	”	6507–7828	3.8	76	”	”	3 × 1200
30 Doradus	”	3800–8400	11	76	”	”	60, 300, 600
LMC N11B	95/12/16	3635–4145	2	−57	04 56 47.0	−66 25 11	600
LMC N11B	”	4060–4520	2	−57	”	”	2 × 1800
LMC N11B	”	4515–4975	2	−57	”	”	2 × 1800
LMC N11B	”	6507–7828	3.8	−57	”	”	600
LMC N11B	”	3800–8400	11	−57	”	”	600
SMC N66	95/12/16	3635–4145	2	−57	00 58 55.2	−72 12 32	600
SMC N66	”	4060–4520	2	−57	”	”	2 × 1800
SMC N66	”	4515–4975	2	−57	”	”	2 × 1800
SMC N66	”	6507–7828	3.8	−57	”	”	600
SMC N66	”	3800–8400	11	−57	”	”	300, 600

order at a resolution of 8.5 Å. The CCD was again binned by a factor of 2 along the slit direction, yielding a plate scale of 1.54 arcsec per pixel.

The Magellanic Cloud H II regions 30 Doradus, LMC N11B and SMC N66 were observed with the NTT 3.5-m telescope in 1995 December. The ESO Multi Mode Instrument was used in the following modes: red imaging and low dispersion grism spectroscopy (RILD) and dichroic medium dispersion spectroscopy (DIMD). The detector was a TEK 1024 × 1024, 24×24 μm^2 CCD (no 31), used for blue-arm DIMD observations, and a TEK 2048 × 2048, 24×24 μm^2 CCD (no 36), used for red-arm DIMD and RILD observations. Both cameras were in use when observing in DIMD mode. In this case, a dichroic prism was inserted into the beam path so that light was directed to the blue and red grating units in synchronization, allowing simultaneous exposures to be obtained in the blue and red parts of the optical spectrum. For all exposures, both CCDs were binned by a factor of 2 in both directions. The spatial sampling was thus 0.74 and 0.54 arcsec per pixel projected on the sky, for CCDs no 31 and no 36, respectively. Five wavelength regions were observed with two different gratings (#3, #7) and a grism (#3), yielding spectral resolutions of approximately 2 Å (λλ3635–4145, λλ4060–4520, λλ4515–4975), 3.8 Å (λλ6507–7828), and 11 Å FWHM (λλ3800–8400), respectively. An OG530 filter was used when observing in DIMD mode. The slits used were 5.6 arcmin long and 1.0 and 1.5 arcsec wide. Relevant exposure times, position angles and target coordinates are listed in Table 1.

The two-dimensional spectra were reduced with the MIDAS software package, following standard procedures. They were bias-subtracted, flat-fielded via division by normalized flat-field frames, cosmic-ray cleaned, and then wavelength calibrated using exposures of He–Ar, Th–Ar and Cu–Ar calibration lamps. During the 1995 and 1997 runs, twilight sky flat-fields were also obtained, in order to correct the small variations in illumination along the slit. The ESO 1.52-m spectra were reduced to absolute intensity units using wide-slit (8 arcsec) observations of the *HST* standard stars Feige 110 and the nucleus of the planetary nebula NGC 7293 (Walsh 1993), as well as the CTIO standards LTT 4364 and LTT 6248 (Hamuy et al. 1994). All NTT spectra were flux-calibrated using wide-slit (5 arcsec) observations of Feige 110. The AAT spectra were flux-calibrated using observations of the standard star LTT 3218. In all cases, flux-calibration was carried out using the IRAF software package. Sky-subtraction was not attempted because in no case could any nebular emission-free windows be extracted from the long-slit CCD frames.

Most of the line fluxes – and certainly all those of heavy-element recombination lines – were derived using Gaussian line profile fitting techniques, apart from the strongest ones, for which their fluxes were measured by simply integrating over the line profiles. In order to deconvolve features affected by blending, multiple Gaussian fitting was employed. In such cases, a successful estimate of the continuum emission level was deemed to be an important first step. After subtracting the local continuum, line fluxes were retrieved by fitting multiple Gaussians of appropriate central wavelength and usually equal FWHM. The FWHM was taken to be the same as that of nearby unblended lines of similar strength to those fitted. Their relative wavelength spacings were constrained to be the same as those from laboratory wavelengths. This procedure ensured accurate flux retrieval and aided line identification in the case of ambiguous features. In Fig. 1 we present high-resolution, continuum-subtracted spectra of 30 Doradus and NGC 3576 covering the spectral region around the O II V1 multiplet at 4650 Å, along with multiple Gaussian fits to the observed emission lines.

A complete list of observed emission lines and their fluxes for all nebulae can be found in Table 2. All fluxes are on a scale where $F(\mathrm{H}\beta) = 100$, with the dereddened flux given by,

$$I(\lambda) = 10^{c(\mathrm{H}\beta)f(\lambda)}\, F(\lambda).$$

The amount of interstellar extinction is given by $c(\mathrm{H}\beta)$ which is the logarithm of the ratio of the dereddened and observed Hβ fluxes,

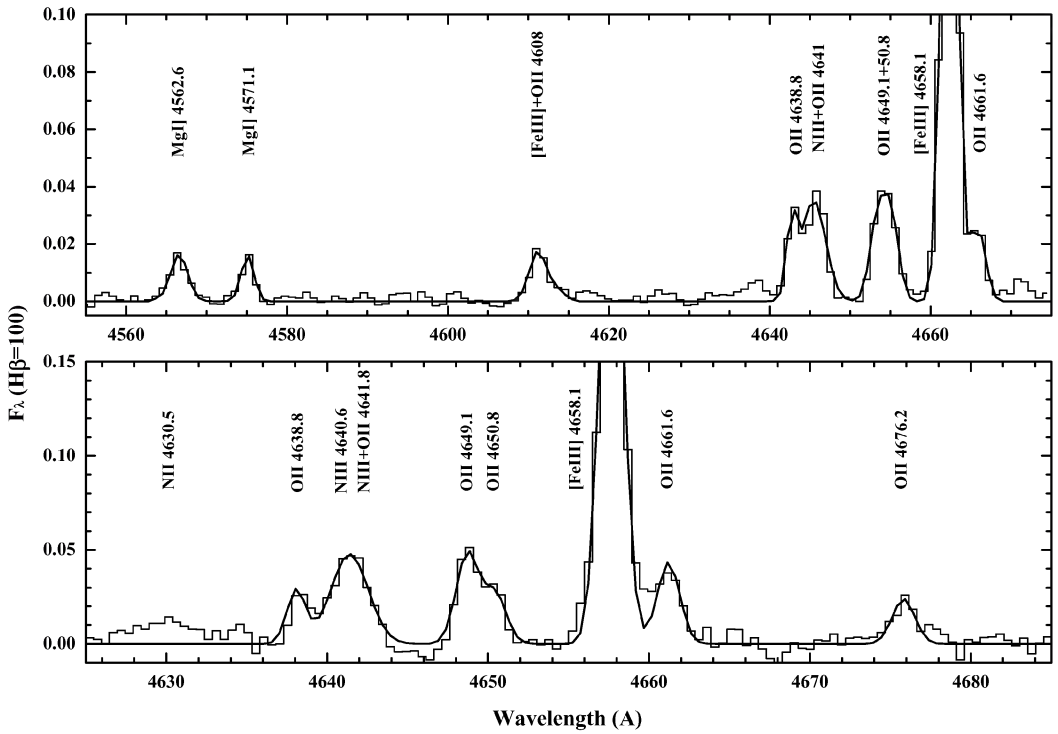

Figure 1. Continuum subtracted spectra of 30 Doradus (top panel, NTT 3.5 m, FWHM = 2 Å) and NGC 3576 (bottom panel, ESO 1.52 m, FWHM = 1.5 Å) showing the O II V1 multiplet recombination lines; interstellar extinction has not been corrected for. The thick overplotted line is the sum of multiple Gaussian fits to the lines. The intensity is scaled to $F(\mathrm{H}\beta) = 100$.

while $f(\lambda)$ is the adopted extinction curve in each case (see below) normalized such that $f(\mathrm{H}\beta) = 0$. A ratio of total to selective extinction, $R = A_V/E(B-V) = 3.1$ was assumed. All dereddened line intensities quoted in the remainder of this paper are on a scale where $I(\mathrm{H}\beta) = 100$.

3 NEBULAR ANALYSIS

3.1 Reddening correction

In the case of the galactic nebulae M 17 and NGC 3576, the galactic reddening law of Howarth (1983) was used to correct for interstellar extinction, with the amount of extinction at Hβ determined by comparing the observed Balmer Hα/Hβ, Hγ/Hβ and Hδ/Hβ decrements to their Case B theoretical values from Storey & Hummer (1995). For the M 17 and NGC 3576 sightlines, values of $c(\mathrm{H}\beta) = 1.84$ and 1.25, respectively, were found.

For the Magellanic Cloud nebulae, the contribution from galactic foreground reddening was estimated from the reddening maps of Burstein & Heiles (1982), using the extinction law of Howarth (1983) in all cases. For the direction to 30 Doradus, $c(\mathrm{H}\beta) = 0.087$ through the Milky Way was found. The remaining extinction due to the immediate 30 Doradus environment was found to be $c(\mathrm{H}\beta) = 0.32$, from the foreground-corrected Balmer decrements, using the LMC extinction law of Howarth (1983). For LMC N11B and SMC N66, no further correction was attempted after foreground Galactic reddenings of $c(\mathrm{H}\beta) = 0.073$ and 0.087, respectively, were corrected for, because the resulting Balmer line ratios were in good agreement with their Case B theoretical values.

3.2 Electron temperatures and densities

Nebular electron temperatures T_e and densities N_e were derived from several CEL diagnostic ratios by solving the equations of statistical equilibrium using the multi-level ($\geqslant$5) atomic model EQUIB; these are presented in Table 3. The atomic data sets used for this purpose, as well as for the derivation of abundances, are the same as those used by Liu et al. (2000) in the study of the planetary nebula NGC 6153. The procedure was as follows. A representative initial T_e of 9000 K was assumed in order to derive N_e(Cl III) and N_e(Ar IV); the mean electron density derived from these diagnostics was then used to derive T_e(O III), and we then iterated once to obtain the final values. In a similar manner, T_e(N II) was derived in conjunction with N_e(O II) and N_e(S II). The Balmer jump (BJ) electron temperatures of M 17 and NGC 3576 were derived from the ratio of the H I recombination continuum Balmer discontinuity at 3646 Å to the H11 λ3770 line. These temperatures are presented in Table 3, along with the mean nebular temperature, T_0, and temperature fluctuation parameter, t^2 (Peimbert 1967) implied by the BJ and [O III] temperatures.

The electron temperatures deduced from the [N II] nebular to auroral line ratio are higher than those of the corresponding [O III] line ratio – except for LMC N11B, where the derived values are probably consistent within the errors. The differences exceed 2000 K for 30 Doradus and SMC N66. Using photoionization models of metal-rich H II regions, Stasińska (1980) has argued that the electron temperature increases outward as a function of radius, probably due to a combination of hardening of the radiation field with increasing optical depth, plus stronger cooling from fine-structure lines of [O III] in the inner parts of the nebulae where O^{2+} dominates; thus,

Table 2. Observed and dereddened relative line fluxes ($F(\lambda)$ and $I(\lambda)$, respectively), on a scale where H$\beta = 100$.

λ_{obs}	$F(\lambda)$	$I(\lambda)$	ID	λ_0	Mult
		M 17			
*	*	*	H 14	3721.94	H 14
*	*	*	[S III]	3721.63	F2
3726.99	3.11(+1)	9.24(+1)	[O II]	3726.03	F1
*	*	*	[O II]	3728.82	F1
3749.86	1.13	3.32	H 12	3750.15	H 12
3770.34	1.31	3.78	H 11	3770.63	H 11
3797.30	1.61	4.53	H 10	3797.90	H 10
3819.01	4.13(−1)	1.14	He I	3819.62	V22
3834.78	2.41	6.59	H 9	3835.39	H9
3868.84	6.91	1.83(+1)	[Ne III	3868.75	F1
3889.14	6.23	1.62(+1)	He I	3888.65	V2
3967.56	8.24	2.01(+1)	[Ne III	3967.46	F1
4009.31	1.26(−1)	2.97(−1)	He I	4009.26	V55
4026.29	9.73(−1)	2.25	He I	4026.21	V18
4069.00	2.60(−1)	5.79(−1)	[S II]	4068.60	F1
4076.23	7.05(−2)	1.56(−1)	[S II]	4076.35	F1
4101.76	1.19(+1)	2.57(+1)	H6	4101.74	H6
4119.71	5.44(−2)	1.15(−1)	O II	4119.22	V20
4121.33	9.00(−2)	1.91(−1)	He I	4120.84	V16
4143.87	1.35(−1)	2.80(−1)	He I	4143.76	V53
4267.19	2.61(−1)	4.81(−1)	C II	4267.15	V6
4317.27	6.36(−2)	1.12(−1)	O II	4317.14	V2
4319.48	1.89(−2)	3.30(−2)	O II	4319.63	V2
4340.43	2.79(+1)	4.77(+1)	H 5	4340.47	H5
	3.93(−2)	6.70(−2)	O II	4345.56	V2
4349.01	6.30(−2)	1.07(−1)	O II	4349.43	V2
4363.22	6.11(−1)	1.02	[O III]	4363.21	F2
4388.02	4.06(−1)	6.63(−1)	He I	4387.93	V51
4437.83	5.37(−2)	8.33(−2)	He I	4437.55	V50
4471.49	3.28	4.91	He I	4471.50	V14
4607.46	4.56(−2)	5.95(−2)	N II	4607.16	V5
4630.76	5.22(−2)	6.02(−2)	N II	4630.54	V5
4634.26	3.42(−2)	4.34(−2)	N III	4634.14	V2
4638.98	8.36(−2)	1.06(−1)	O II	4638.49	V1
4640.76	2.77(−2)	3.48(−2)	N III	4640.64	V2
4641.93	1.28(−1)	1.52(−1)	O II	4641.44	V1
4649.38	1.10(−1)	1.38(−1)	O II	4649.13	V1
4651.09	6.99(−2)	8.71(−2)	O II	4650.84	V1
4658.49	2.25(−1)	2.79(−1)	[Fe III]	4658.10	F3
4662.02	8.47(−2)	1.04(−1)	O II	4661.63	V1
4676.91	5.19(−2)	6.30(−2)	O II	4676.24	V1
4711.60	7.01(−2)	8.20(−2)	[Ar IV]	4711.37	F1
4713.40	4.51(−1)	5.26(−1)	He I	4713.17	V12
4740.37	6.20(−2)	7.04(−2)	[Ar IV]	4740.17	F1
4803.20	2.85(−2)	3.04(−2)	N II	4803.29	V20
4861.55	1.00(+2)	1.00(+2)	H4	4861.33	H4
4881.20	1.04(−1)	1.02(−1)	[Fe III]	4881.11	F2
4906.87	5.42(−2)	5.17(−2)	O II	4906.83	V28
4922.27	1.42	1.34	He I	4921.93	V48
4931.47	4.49(−2)	4.18(−2)	[O III]	4931.80	F1
4959.13	1.30(+2)	1.17(+2)	[O III]	4958.91	F1
5006.43	4.13(+2)	3.55(+2)	[O III]	5006.84	F1
5198.36	4.04(−1)	2.84(−1)	[N I]	5199.84	F1
5517.48	8.73(−1)	4.54(−1)	[Cl III]	5517.66	F1
5537.71	7.75(−1)	3.97(−1)	[Cl III]	5537.60	F1
5666.60	1.23(−1)	5.70(−2)	N II	5666.53	V3
5676.11	3.68(−2)	1.70(−2)	N II	5676.02	V3
5679.62	1.18(−1)	5.44(−2)	N II	5679.56	V3
5754.74	7.40(−1)	3.24(−1)	[N II]	5754.60	F3
5875.44	3.61(+1)	1.45(+1)	He I	5875.66	V11
6312.09	4.77	1.43	[S III]	6312.10	F3
6548.71	3.52(+1)	9.15	[N II]	6548.10	F1
6563.11	1.17(+3)	3.01(+2)	H3	6562.77	H3
6583.91	1.08(+2)	2.74(+1)	[N II]	6583.50	F1
6678.59	1.62(+1)	3.89	He I	6678.16	V46
6717.02	1.72(+1)	4.04	[S II]	6716.44	F2
6731.39	1.76(+1)	4.11	[S II]	6730.82	F2
7065.48	1.81(+1)	3.51	He I	7065.25	V10
7135.90	5.74(+1)	1.07(+1)	[Ar III]	7135.80	F1
7280.02	5.49	9.50(−1)	He I	7281.35	V45
7319.06	6.61	1.12	[O II]	7318.92	F2
7329.62	5.17	8.72(−1)	[O II]	7329.67	F2
		NGC 3576 (AAT)			
3531.25	3.98(−1)	9.70(−1)	He I	3530.50	V36
3553.94	1.55(−1)	3.71(−1)	He I	3554.42	V34
3566.73	4.25(−1)	1.00	?	3566.95	
3613.22	2.17(−1)	4.92(−1)	He I	3613.64	V6
3634.00	2.30(−1)	5.13(−1)	He I	3634.25	V28
3671.17	2.34(−1)	5.13(−1)	H 24	3671.48	H 24
3673.39	2.24(−1)	4.90(−1)	H 23	3673.74	H 23
3676.01	2.80(−1)	6.11(−1)	H 22	3676.36	H 22
3679.01	2.87(−1)	6.26(−1)	H 21	3679.36	H 21
3682.46	3.17(−1)	6.92(−1)	H 20	3682.81	H 20
3686.48	3.70(−1)	8.04(−1)	H 19	3686.83	H 19
3691.21	4.42(−1)	9.59(−1)	H 18	3691.56	H 18
3696.80	4.91(−1)	1.06	H 17	3697.15	H 17
3703.50	6.09(−1)	1.31	H 16	3703.86	H 16
3704.66	3.01(−1)	6.49(−1)	He I	3705.02	V25
3711.61	7.40(−1)	1.58	H 15	3711.97	H 15
3721.49	1.31	2.79	H 14	3721.94	H 14
3725.66	3.52(+1)	7.51(+1)	[O II]	3726.03	F1
3728.45	2.58(+1)	5.49(+1)	[O II]	3728.82	F1
3733.99	1.05	2.23	H 13	3734.37	H 13
3749.77	1.38	2.90	H 12	3750.15	H 12
3770.25	1.80	3.76	H 11	3770.63	H 11
3797.52	2.51	5.16	H 10	3797.90	H 10
3819.21	5.86(−1)	1.18	He I	3819.62	V22
3835.00	3.75	7.54	H 9	3835.39	H9
3855.69	1.22(−1)	2.44(−1)	Si II	3856.02	V1
3862.27	1.43(−1)	2.83(−1)	Si II	3862.60	V1
3868.34	1.04(+1)	2.06(+1)	[Ne III]	3868.75	F1
3871.33	8.97(−2)	1.76(−1)	He I	3871.82	V60
3888.64	8.45	1.64(+1)	He I	3888.65	V2
3912.83	3.95(−2)	7.59(−2)	?	3912.83	
3914.02	3.39(−2)	6.52(−2)	?	3914.02	
3918.66	5.39(−2)	1.03(−1)	C II	3918.98	V4
3920.37	4.83(−2)	9.24(−2)	C II	3920.69	V4
3926.03	8.01(−2)	1.52(−1)	He I	3926.54	V58
3964.36	4.81(−1)	8.97(−1)	He I	3964.73	V5
3967.04	3.20	5.95	[Ne III]	3967.46	F1
3969.70	8.03	1.49(+1)	H 7	3970.07	H7
4008.84	1.27(−1)	2.31(−1)	He I	4009.26	V55
4025.83	1.11	2.00	He I	4026.21	V18
4037.19	1.24(−2)	2.22(−2)	?	4037.19	
4042.91	2.56(−2)	4.54(−2)	?	4042.91	
4059.17	1.37(−2)	2.41(−2)	?	4059.17	
4060.28	9.18(−3)	1.61(−2)	[F IV]	4060.23	F1
4065.35	2.37(−2)	4.14(−2)	?	4065.35	
4068.21	7.35(−1)	1.28	[S II]	4068.60	F1
4069.37	8.08(−2)	1.41(−1)	O II	4069.62	V10
			O II	4069.89	V10
4071.77	6.93(−2)	1.21(−1)	O II	4072.16	V10
4075.47	5.81(−2)	1.01(−1)	O II	4075.86	V10
4075.96	2.53(−1)	4.40(−1)	[S II]	4076.35	F1
4080.81	1.95(−2)	3.38(−2)	?	4080.81	

Table 2 – *continued*

λ_{obs}	$F(\lambda)$	$I(\lambda)$	ID	λ_0	Mult
4084.90	9.84(−3)	1.70(−2)	O II	4085.11	V10
4086.93	2.40(−2)	4.15(−2)	O II	4087.15	V48c
4089.07	1.85(−2)	3.20(−2)	O II	4089.29	V48a
4096.94	3.79(−2)	6.50(−2)	N III	4097.33	V1
4101.33	1.50(+1)	2.56(+1)	H 6	4101.74	H 6
4118.83	1.61(−2)	2.71(−2)	O II	4119.22	V20
4120.45	1.26(−1)	2.13(−1)	He I	4120.84	V16
4132.64	3.12(−2)	5.23(−2)	O II	4132.80	V19
4143.33	1.85(−1)	3.07(−1)	He I	4143.76	V53
4152.88	2.18(−2)	3.61(−2)	O II	4153.30	V19
4156.11	1.26(−2)	2.08(−2)	O II	4156.53	V19
4168.62	4.03(−2)	6.58(−2)	He I	4168.97	V52
4170.28	1.94(−2)	3.16(−2)	?	4170.28	
4185.44	2.04(−2)	3.30(−2)	O II	4185.45	V36
4189.78	1.95(−2)	3.14(−2)	O II	4189.79	V36
4253.66	2.72(−2)	4.20(−2)	O II	4254.00	V101
4266.73	2.12(−1)	3.24(−1)	C II	4267.15	V6
4276.78	8.81(−2)	1.34(−1)	O II	4275.55	V67a
4287.00	7.39(−2)	1.11(−1)	[Fe II]	4287.40	7F
4340.04	3.27(+1)	4.76(+1)	H 5	4340.47	H5
4345.30	7.48(−2)	1.08(−1)	O II	4345.56	V2
4349.17	5.38(−2)	7.77(−2)	O II	4349.43	V2
4357.14	5.26(−2)	7.56(−2)	O II	4357.25	V63a
4358.98	8.28(−2)	1.18(−1)	?	4358.98	
4362.80	1.05	1.51	[O III]	4363.21	F2
4368.06	7.49(−2)	1.06(−1)	C II?	4368.14	V45
4387.49	3.91(−1)	5.50(−1)	He I	4387.93	V51
4413.23	7.58(−2)	1.04(−1)	[Fe II]	4413.78	7F
4471.07	3.66	4.84	He I	4471.50	V14
4603.76	3.33(−2)	4.01(−2)	?	4603.76	
4606.98	4.78(−2)	5.75(−2)	N II	4607.16	V5
4608.66	4.45(−2)	5.34(−2)	?	4608.66	
4610.02	4.50(−2)	5.40(−2)	O II	4610.20	V92c
4614.92	4.04(−2)	4.83(−2)	?	4614.92	
4620.88	3.82(−2)	4.55(−2)	N II	4621.39	V5
4638.46	5.89(−2)	6.92(−2)	O II	4638.86	V1
4640.24	2.19(−2)	2.57(−2)	N III	4640.64	V2
4641.42	9.22(−2)	1.08(−1)	O II	4641.81	V1
4648.60	1.38(−1)	1.60(−1)	O II	4649.13	V1
4650.31	1.31(−1)	1.52(−1)	O II	4650.84	V1
4661.23	7.46(−2)	8.61(−2)	O II	4661.63	V1
4675.84	5.12(−2)	5.85(−2)	O II	4676.24	V1
4696.03	2.80(−2)	3.16(−2)	O II	4696.35	V1
4701.16	1.92(−1)	2.16(−1)	[Fe III]	4701.62	F3
4705.72	3.76(−2)	4.21(−2)	O II	4705.35	V25
4861.50	1.00(+2)	1.00(+2)	H 4	4861.33	H4
4958.86	1.31(+2)	1.22(+2)	[O III]	4958.91	F1
5006.82	4.12(+2)	3.71(+2)	[O III]	5006.84	F1
5200.35	8.17(−1)	6.40(−1)	[N I]	5199.84	F1
5270.91	4.51(−1)	3.36(−1)	[Fe III]	5270.40	1F
5518.20	7.41(−1)	4.70(−1)	[Cl III]	5517.66	F1
5538.14	8.49(−1)	5.33(−1)	[Cl III]	5537.60	F1
5577.88	4.18	2.57	[O I]	5577.34	F3
5666.60	6.00(−2)	3.58(−2)	N II	5666.53	V3
5676.11	2.67(−1)	1.59(−2)	N II	5676.02	V3
5679.60	1.12(−1)	6.70(−2)	N II	5679.56	V3
5754.86	1.05	5.92(−1)	[N II]	5754.60	F3
5875.76	2.59(+1)	1.38(+1)	He I	5875.66	V11
5913.00	6.56(−2)	3.42(−2)	?	5913.00	
5931.52	2.11(−1)	1.09(−1)	N II	5931.52	V28
5957.35	2.87(−1)	1.46(−1)	Si II	5957.35	
5978.71	1.99(−1)	1.01(−1)	Si II	5978.71	
6548.11	4.03(+1)	1.58(+1	[N II]	6548.10	F1
6562.97	7.40(+2)	2.88(+2)	H3	6562.77	H3
6583.66	1.36(+2)	5.25(+1)	[N II]	6583.50	F1

Table 2 – *continued*

λ_{obs}	$F(\lambda)$	$I(\lambda)$	ID	λ_0	Mult
6678.74	9.91	3.68	He I	6678.16	V46
6717.02	1.90(+1)	6.94	[S II]	6716.44	F2
6731.40	2.41(+1)	8.76	[S II]	6730.82	F2
7065.67	1.70(+1)	5.45	He I	7065.25	V10
7136.12	4.87(+1)	1.51(+1)	[Ar III]	7135.80	F1
		NGC 3576 (ESO)			
4008.73	1.41(−1)	2.52(−1)	He I	4009.26	V55
4025.77	1.07	1.89	He I	4026.21	V18
4068.12	8.95(−1)	1.54	[S II]	4068.60	F1
4075.73	3.30(−1)	5.65(−1)	[S II]	4076.35	F1
4101.16	1.50(+1)	2.53(+1)	H 6	4101.74	H 6
4120.36	1.26(−1)	2.10(−1)	He I	4120.84	V16
4143.17	1.04(−1)	1.71(−1)	He I	4143.76	V53
4266.58	2.06(−1)	3.12(−1)	C II	4267.15	V6
4276.29	4.80(−2)	7.21(−2)	O II	4275.99	V67b
4286.98	7.73(−2)	1.15(−1)	O II	4285.69	V78b
4316.94	1.23(−1)	1.80(−1)	O II	4317.14	V2
4339.87	3.25(+1)	4.68(+1)	H 5	4340.47	H5
4349.02	3.38(−2)	4.84(−2)	O II	4349.43	V2
4362.64	8.61(−1)	1.22	[O III]	4363.21	F2
4367.45	8.59(−2)	1.21(−1)	O II	4366.89	V2
4387.39	3.18(−1)	4.44(−1)	He I	4387.93	V51
4412.28	5.20(−2)	7.13(−2)	Ne II	4413.22	V65
4413.96	4.55(−2)	6.22(−2)	O II	4414.90	V5
4416.03	5.81(−2)	7.94(−2)	O II	4416.97	V5
4437.45	5.83(−2)	7.84(−2)	He I	4437.55	V50
4449.91	2.49(−2)	3.33(−2)	?	4449.91	
4451.61	4.05(−2)	5.40(−2)	O II	4452.37	V5
4470.93	3.24	4.27	He I	4471.50	V14
4630.03	2.34(−2)	3.09(−2)	N II	4630.54	V5
4638.79	4.34(−2)	5.09(−2)	O II	4638.49	V1
4640.57	3.61(−2)	4.22(−2)	N III	4640.64	V2
4641.74	7.54(−2)	8.80(−2)	O II	4641.44	V1
4648.70	8.00(−2)	9.29(−2)	O II	4649.13	V1
4650.41	4.76(−2)	5.53(−2)	O II	4650.84	V1
4657.68	5.10(−1)	5.89(−1)	[Fe III]	4658.10	F3
4661.21	7.95(−2)	9.16(−2)	O II	4661.63	V1
4675.90	4.91(−2)	5.60(−2)	O II	4676.24	V1
4701.14	1.60(−1)	1.79(−1)	[Fe III]	4701.62	F3
4710.98	7.82(−2)	8.70(−2)	[Ar IV]	4711.37	F1
4712.78	4.43(−1)	4.91(−1)	He I	4713.17	V12
4733.55	4.13(−2)	4.52(−2)	[Fe III]	4733.93	
4739.65	6.92(−2)	7.54(−2)	[Ar IV]	4740.17	F1
4754.43	1.01(−1)	1.09(−1)	[Fe III]	4754.83	
4860.93	1.00(+2)	1.00(+2)	H 4	4861.33	H4
4880.75	2.26(−1)	2.23(−1)	[Fe III]	4881.11	F2
4921.62	1.12	1.07	He I	4921.93	V48
4924.22	6.68(−2)	6.39(−2)	O II	4924.53	V28
4930.97	8.22(−2)	7.82(−2)	[O III]	4931.80	F1
4958.53	1.25(+2)	1.17(+2)	[O III]	4958.91	F1
		30 Doradus			
3729.15	3.80(+1)	5.02(+1)	[O II]	3726.03	F1
3731.94	4.21(+1)	5.54(+1)	[O II]	3728.82	F1
3753.37	2.69	3.52	H 12	3750.15	H 12
3773.87	3.29	4.28	H 11	3770.63	H 11
3801.17	4.35	5.61	H 10	3797.90	H 10
3822.94	9.27(−1)	1.18	He I	3819.62	V22
3838.69	6.48	8.26	H 9	3835.39	H9
3871.99	3.07(+1)	3.87(+1)	[Ne III]	3868.75	F1
3892.31	1.55(+1)	1.94(+1)	He I	3888.65	V2
3970.79	9.37	1.14(+1)	[Ne III]	3967.46	F1
3973.40	1.40(+1)	1.71(+1)	H7	3970.07	H7
4072.50	4.71(−1)	5.61(−1)	[S II]	4068.60	F1

Table 2 – *continued*

λ_{obs}	$F(\lambda)$	$I(\lambda)$	ID	λ_0	Mult
4073.66	1.11(−1)	1.33(−1)	O II	4069.62	V10
4076.06	5.73(−2)	6.83(−2)	O II	4072.16	V10
4080.26	1.90(−1)	2.27(−1)	[S II]	4076.35	F1
4082.75	2.73(−2)	3.24(−2)	O II	4078.84	V10
4087.98	9.11(−3)	1.08(−2)	O II	4083.90	V48b
4089.20	2.17(−2)	2.58(−2)	O II	4085.11	V10
4091.24	1.56(−2)	1.85(−2)	O II	4087.15	V48c
4093.38	1.77(−2)	2.10(−2)	O II	4089.29	V48a
4105.56	2.20(+1)	2.60(+1)	H 6	4101.74	H 6
4114.32	2.74(−2)	3.22(−2)	O II	4110.78	V20
4124.62	1.77(−1)	2.08(−1)	He I	4120.84	V16
4136.45	4.33(−2)	5.08(−2)	O II	4132.80	V19
4147.48	2.52(−1)	2.94(−1)	He I	4143.76	V53
4156.82	5.22(−2)	6.09(−2)	O II	4153.30	V19
4160.05	1.99(−2)	2.32(−2)	O II	4156.53	V19
4172.75	5.74(−2)	6.66(−2)	O II	4169.22	V19
4270.73	8.11(−2)	9.19(−2)	C II	4267.15	V6
4279.08	6.94(−2)	7.85(−2)	O II	4275.55	V67a
4307.40	4.62(−2)	5.19(−2)	O II	4303.61	V65a
4314.99	2.64(−2)	2.96(−2)	O II	4312.11	V78a
4315.49	3.42(−2)	3.83(−2)	O II	4313.44	V78a
4317.45	2.46(−2)	5.33(−2)	O II	4315.40	V63c
4319.19	6.30(−2)	7.05(−2)	O II	4317.14	V2
4321.68	7.83(−2)	8.76(−2)	O II	4319.63	V2
4344.22	4.35(+1)	4.84(+1)	H 5	4340.47	H5
4367.00	3.03	3.35	[O III]	4363.21	F2
4391.79	4.87(−1)	5.36(−1)	He I	4387.93	V51
4412.55	2.83(−2)	3.10(−2)	Ne II	4409.30	V55e
4418.15	3.03(−2)	3.32(−2)	O II	4414.90	V5
4420.23	3.98(−2)	4.36(−2)	O II	4416.97	V5
4441.41	5.71(−2)	6.22(−2)	He I	4437.55	V50
4475.44	4.03	4.35	He I	4471.50	V14
4566.56	4.77(−2)	5.06(−2)	Mg I]	4562.60	
4575.32	5.39(−2)	5.70(−2)	Mg I]	4571.10	
4611.30	4.82(−2)	5.06(−2)	[Fe III]	4607.13	3F
4613.96	1.99(−2)	2.09(−2)	O II	4609.44	V92a
4638.92	9.71(−3)	1.01(−2)	N III	4634.14	V2
4643.03	6.13(−2)	6.40(−2)	O II	4638.49	V1
4645.99	8.19(−2)	8.54(−2)	O II	4641.81	V1
4653.38	6.16(−2)	6.42(−2)	O II	4649.13	V1
4655.09	6.16(−2)	6.41(−2)	O II	4650.84	V1
4662.27	6.01(−1)	6.25(−1)	[Fe III]	4658.10	3F
4665.18	5.44(−2)	5.65(−2)	O II	4661.63	V1
4671.08	2.26(−2)	2.35(−2)	[Fe III]	4667.00	3F
4677.91	1.16(−2)	1.20(−2)	O II	4673.73	V1
4680.42	2.15(−2)	2.24(−2)	O II	4676.24	V1
4689.06	1.66(−2)	1.71(−2)	He II	4685.68	3.4
4692.90	1.09(−2)	1.12(−2)	?	4692.90	
4696.27	1.71(−2)	1.77(−2)	?	4696.27	
4705.74	1.83(−1)	1.88(−1)	[Fe III]	4701.62	3F
4715.54	2.04(−1)	2.10(−1)	[Ar IV]	4711.37	F1
4717.34	4.67(−1)	4.80(−1)	He I	4713.17	V12
4738.18	6.17(−2)	6.31(−2)	[Fe III]	4733.93	3F
4744.40	1.77(−1)	1.81(−1)	[Ar IV]	4740.17	F1
4753.57	1.87(−2)	1.91(−2)	?	*	
4758.89	1.35(−1)	1.38(−1)	[Fe III]	4754.83	3F
4773.70	6.67(−2)	6.79(−2)	[Fe III]	4769.60	3F
4781.58	3.16(−2)	3.21(−2)	[Fe III]	4777.88	3F
4800.53	1.85(−2)	1.87(−2)	?	*	
4819.44	3.05(−2)	3.07(−2)	[Fe II]	4814.55	20F
4865.59	1.00(+2)	1.00(+2)	H 4	4861.33	H4
4885.14	1.83(−1)	1.83(−1)	[Fe III]	4881.11	2F
4893.48	1.72(−2)	1.71(−2)	[Fe II]	4889.63	4F
4907.18	3.37(−2)	3.35(−2)	[Fe IV]	4903.50	-F

Table 2 – *continued*

λ_{obs}	$F(\lambda)$	$I(\lambda)$	ID	λ_0	Mult
4910.38	3.72(−2)	3.69(−2)	O II	4906.83	V28
4926.27	1.16	1.14	He I	4921.93	V48
4935.46	7.03(−2)	6.94(−2)	[O III]	4931.80	F1
4967.44	1.71(+2)	1.68(+2)	[O III]	4958.91	F1
5015.56	5.18(+2)	5.05(+2)	[O III]	5006.84	F1
5279.65	2.99(−1)	2.79(−1)	[Fe II]	5273.38	18F
5315.59	1.71(−1)	1.58(−1)	?	*	
5526.27	5.28(−1)	4.76(−1)	[Cl III]	5517.66	F1
5546.24	4.10(−1)	3.69(−1)	[Cl III]	5537.60	F1
5762.29	2.35(−1)	2.06(−1)	[N II]	5754.60	F3
5883.20	1.48(+1)	1.27(+1)	He I	5875.66	V11
6238.42	1.75(−1)	1.45(−1)	[Ni III]	6231.09	
6261.66	1.53(−1)	1.26(−1)	[Fe II]	6254.30	
6306.34	1.30	1.07	[O I]	6300.34	F1
6318.12	2.37	1.94	[S III]	6312.10	F3
6562.58	4.04	3.22	[N II]	6548.10	F1
6576.15	3.80(+2)	3.03(+2)	H 3	6562.77	H3
6595.37	1.09(+1)	8.73	[N II]	6583.50	F1
6685.50	4.64	3.65	He I	6678.16	V46
6722.67	7.66	6.00	[S II]	6716.44	F2
6736.74	6.94	5.43	[S II]	6730.82	F2
7074.23	4.69	3.55	He I	7065.25	V10
7146.92	1.80(+1)	1.35(+1)	[Ar III]	7135.80	F1
7166.65	4.65(−2)	3.49(−2)	[Fe II]	7155.14	14F
7247.38	3.26(−1)	2.43(−1)	C II	7231.32	V3
7252.50	3.41(−1)	2.54(−1)	C II	7236.42	V3
7296.23	9.94(−1)	7.38(−1)	He I	7281.35	V45
7335.88	2.80	2.07	[O II]	7318.92	F2
7346.65	2.30	1.70	[O II]	7329.67	F2
			LMC N11B		
3729.14	7.92(+1)	8.27(+1)	[O II]	3726.03	F1
3731.94	1.05(+2)	1.10(+2)	[O II]	3728.82	F1
3872.02	1.97(+1)	2.05(+1)	[Ne III]	3868.75	F1
3892.03	2.15(+1)	2.23(+1)	He I	3888.65	V2
3970.38	3.38	3.50	[Ne III]	3967.46	F1
3973.23	1.35(+1)	1.40(+1)	H 7	3970.07	H7
4072.97	8.37(−1)	8.64(−1)	[S II]	4068.60	F1
4074.13	3.07(−1)	3.17(−1)	O II	4069.62	V10
4076.53	9.94(−2)	1.03(−1)	O II	4072.16	V10
4080.73	4.89(−1)	5.05(−1)	[S II]	4076.35	F1
4083.22	1.61(−1)	1.67(−1)	O II	4078.84	V10
4086.71	1.36(−1)	1.41(−1)	?	4086.71	
4088.71	1.49(−1)	1.54(−1)	O II	4083.90	V48b
4089.92	1.05(−1)	1.09(−1)	O II	4085.11	V10
4091.97	1.10(−1)	1.13(−1)	O II	4087.15	V48c
4094.11	1.26(−1)	1.31(−1)	O II	4089.29	V48a
4106.03	2.68(+1)	2.77(+1)	H 6	4101.74	H 6
4114.41	1.51(−1)	1.56(−1)	O II	4110.78	V20
4116.86	1.44(−1)	1.49(−1)	?	4116.86	
4125.03	2.74(−1)	2.82(−1)	He I	4120.84	V16
4135.89	1.08(−1)	1.11(−1)	O II	4129.32	V19
4139.38	1.32(−1)	1.36(−1)	O II	4132.80	V19
4147.96	3.07(−1)	3.16(−1)	He I	4143.76	V53
4157.64	9.54(−2)	9.82(−2)	O II	4153.30	V19
4160.87	1.24(−1)	1.28(−1)	O II	4156.53	V19
4164.34	2.30(−1)	2.37(−1)	?	4164.34	
4169.09	2.29(−1)	2.35(−1)	?	4169.09	
*	*	*	O II	4169.22	V19
4179.89	8.61(−2)	8.85(−2)	N II	4176.16	V43a
4190.33	8.63(−2)	8.87(−2)	C III]	4186.90	V18
4193.23	1.51(−1)	1.55(−1)	O II	4189.79	V36
4207.42	1.29(−1)	1.32(−1)	?	4207.42	
4212.17	3.90(−1)	4.00(−1)	?	4212.17	

Table 2 – *continued*

λ_{obs}	$F(\lambda)$	$I(\lambda)$	ID	λ_0	Mult
4218.52	1.15(−1)	1.18(−1)	?	4218.52	
4221.32	1.75(−1)	1.79(−1)	?	4221.32	
4241.04	9.68(−2)	9.93(−2)	N II	4237.05	
4245.50	2.88(−1)	2.95(−1)	N II	4241.78	V48a
4252.40	2.03(−1)	2.08(−1)	?	4248.15	
4257.04	2.57(−1)	2.64(−1)	?	4252.73	
4263.04	1.94(−1)	1.99(−1)	?	4263.04	
4265.80	2.54(−1)	2.60(−1)	?	4265.80	
4268.90	1.91(−1)	1.95(−1)	C II	4267.15	V6
4277.87	4.16(−1)	4.26(−1)	O II	4276.28	V67b
4282.91	2.61(−1)	2.67(−1)	O II	4281.32	V53b
4287.28	1.07(−1)	1.09(−1)	O II	4285.69	V78b
4292.84	2.73(−1)	2.79(−1)	O II	4291.25	V55
4316.78	3.79(−1)	3.87(−1)	O II	4312.11	V78a
4320.07	7.82(−1)	8.00(−1)	O II	4315.40	V63c
4318.80	1.31(−1)	1.34(−1)	O II	4317.14	V2
4321.01	3.34(−1)	3.41(−1)	O II	4319.63	V2
4329.52	2.86(−1)	2.92(−1)	O II	4325.76	V2
4332.30	1.89(−1)	1.93(−1)	?	4329.08	
4334.89	2.82(−1)	2.88(−1)	O II	4331.13	V65b
4344.77	4.58(+1)	4.67(+1)	H 5	4340.47	H5
4353.52	1.31(−1)	8.71(−2)	O II	4349.43	V2
4357.68	1.31(−1)	1.34(−1)	O II	4353.59	V76c
4367.56	1.65	1.68	[O III]	4363.21	F2
4392.35	4.85(−1)	4.95(−1)	He I	4387.93	V51
4412.04	2.00(−1)	2.04(−1)	?	4412.00	
4419.80	2.18(−1)	2.22(−1)	O II	4414.90	V5
4475.98	4.24	4.31	He I	4471.50	V14
4532.10	4.14(−2)	4.20(−2)	?	4541.25	
4537.53	8.80(−2)	8.92(−2)	?	4537.54	
4539.73	5.77(−2)	5.85(−2)	N III	4534.58	V3
4542.95	7.87(−2)	7.97(−2)	?	4542.95	
4546.93	7.77(−2)	7.87(−2)	?	4546.93	
4560.15	1.49(−1)	1.51(−1)	[Fe II]	4555.00	
4561.54	2.59(−2)	2.63(−2)	Fe II	4556.39	
4567.55	1.92(−1)	1.95(−1)	Mg I]	4562.60	
4576.06	2.01(−1)	2.03(−1)	Mg I]	4571.10	
4589.35	5.92(−2)	5.99(−2)	?	4584.40	
4609.38	4.64(−2)	4.69(−2)	?	4604.43	
4643.65	1.15(−1)	1.17(−1)	O II	4638.49	V1
4646.29	2.73(−2)	2.75(−2)	N III	4640.64	V2
4647.08	5.26(−2)	5.30(−2)	O II	4641.81	V1
4654.05	7.55(−2)	7.60(−2)	O II	4649.13	V1
4655.76	6.27(−2)	6.31(−2)	O II	4650.84	V1
4662.81	2.69(−1)	2.72(−1)	[Fe III]	4658.10	3F
4665.73	7.05(−2)	6.40(−2)	O II	4661.63	V1
4670.96	2.54(−2)	2.56(−2)	[Fe III]	4667.00	3F
4677.69	3.05(−2)	3.08(−2)	O II	4673.73	V1
4686.08	5.00(−2)	5.04(−2)	?	4681.44	
4695.95	8.14(−2)	8.20(−2)	?	4691.31	
4700.84	3.43(−2)	3.46(−2)	O II	4696.35	V1
4706.12	9.02(−2)	9.08(−2)	[Fe III]	4701.62	3F
4711.25	2.60(−2)	2.61(−2)	?	4706.60	
4717.81	5.06(−1)	5.09(−1)	He I	4713.17	V12
4724.58	6.19(−2)	6.23(−2)	?	4719.94	
4732.73	1.83(−2)	1.84(−2)	?	4728.09	
4744.92	1.12(−1)	1.13(−1)	[Ar IV]	4740.17	F1
4749.76	2.41(−2)	2.43(−2)	[Fe II]	4745.48	
4759.60	8.73(−2)	8.77(−2)	[Fe III]	4754.83	3F
4774.42	3.93(−2)	3.94(−2)	[Fe III]	4769.60	3F
4779.56	2.61(−2)	2.62(−2)	[Fe II]	4774.74	20F
4795.55	7.17(−2)	7.19(−2)	?	*	
4803.51	2.18(−2)	2.18(−2)	?	4798.87	
4815.88	6.52(−2)	6.53(−2)	?	4815.88	

Table 2 – *continued*

λ_{obs}	$F(\lambda)$	$I(\lambda)$	ID	λ_0	Mult
4819.93	9.96(−2)	9.98(−2)	[Fe II]	4814.55	20F
4865.95	1.00(+2)	1.00(+2)	H 4	4861.33	H4
4885.52	5.33(−2)	5.32(−2)	[Fe III]	4881.11	2F
4905.47	2.92(−2)	2.91(−2)	[Fe IV]?	4900.50	-F
4926.64	1.08	1.07	He I	4921.93	V48
4929.24	1.26(−1)	1.26(−1)	O II	4924.53	V28
4935.89	7.44(−2)	7.42(−2)	[O III]	4931.80	F1
4968.01	1.10(+2)	1.09(+2)	[O III]	4958.91	F1
5016.07	3.32(+2)	3.30(+2)	[O III]	5006.84	F1
5052.34	1.32(−1)	1.31(−1)	?	5052.34	
5060.59	4.73(−1)	4.69(−1)	?	5060.59	
5526.40	5.07(−1)	4.94(−1)	[Cl III]	5517.66	F1
5546.37	4.94(−1)	4.81(−1)	[Cl III]	5537.60	F1
5752.46	1.23(−1)	1.19(−1)	?	5752.46	
5763.87	2.09(−1)	2.02(−1)	[N II]	5754.60	F3
5883.90	1.52(+1)	1.47(+1)	He I	5875.66	V11
6564.36	6.11	5.79	[N II]	6548.10	F1
6578.06	3.34(+2)	3.16(+2)	H3	6562.77	H3
6597.40	1.75(+1)	1.65(+1)	[N II]	6583.50	F1
6687.50	3.89	3.68	He I	6678.16	V46
6724.72	1.50(+1)	1.42(+1)	[S II]	6716.44	F2
6738.76	1.11(+1)	1.05(+1)	[S II]	6730.82	F2
7076.35	2.48	2.32	He I	7065.25	V10
7149.04	1.23(+1)	1.15(+1)	[Ar III]	7135.80	F1
7158.08	2.67(−1)	2.49(−1)	?	*	
7294.45	1.83	1.71	He I	7281.35	V45
7338.55	4.60	4.28	[O II]	7318.92	F2
7350.41	6.26	5.84	[O II]	7329.67	F2
			SMC N66		
3705.43	2.39	2.52	H 16	3703.86	H 16
3713.54	1.83	1.93	H 15	3711.97	H 15
3723.31	3.55	3.73	[S III]	3721.63	F2
3727.50	4.77(+1)	5.02(+1)	[O II]	3726.03	F1
3730.29	6.80(+1)	7.16(+1)	[O II]	3728.82	F1
3736.06	2.94	3.09	H 13	3734.37	H 13
3751.70	2.83	2.97	H 12	3750.15	H 12
3772.19	3.86	4.05	H 11	3770.63	H 11
3799.47	5.17	5.43	H 10	3797.90	H 10
3836.98	7.27	7.62	H9	3835.39	H9
3870.25	3.72(+1)	3.89(+1)	[Ne III]	3868.75	F1
*	*	*	He I	3888.65	V2
3890.56	1.89(+1)	1.98(+1)	H8	3889.05	H8
3969.00	1.03(+1)	1.07(+1)	[Ne III]	3967.46	F1
3971.61	1.49(+1)	1.56(+1)	H7	3970.07	H7
4027.79	2.38	2.47	He I	4026.21	V18
4071.28	9.37(−1)	9.73(−1)	[S II]	4068.60	F1
4076.17	1.43(−1)	1.49(−1)	?	4073.74	
4079.03	2.85(−1)	2.96(−1)	[S II]	4076.35	F1
4081.53	6.41(−2)	6.65(−2)	O II	4078.84	V10
4104.35	2.58(+1)	2.67(+1)	H 6	4101.74	H 6
4114.66	5.04(−2)	5.23(−2)	?	4112.59	
4123.59	2.51(−1)	2.60(−1)	He I	4120.84	V16
4128.30	7.48(−2)	7.75(−2)	?	4125.62	
4146.25	3.07(−1)	3.18(−1)	He I	4143.76	V53
4155.79	1.07(−1)	1.11(−1)	O II	4153.30	V19
4171.46	9.24(−2)	9.56(−2)	O II	4169.22	V19
4207.77	1.05(−1)	1.08(−1)	?	4204.93	
4342.97	4.61(+1)	4.73(+1)	H5	4340.47	H5
4349.37	5.93(−2)	6.08(−2)	S II	4347.20	
4358.29	6.29(−2)	6.45(−2)	?	4355.74	
4361.93	4.87(−2)	4.99(−2)	[Fe II]	4359.34	7F
4365.70	6.11	6.26	[O III]	4363.21	F2
4390.47	4.61(−1)	4.71(−1)	He I	4387.93	V51

Table 2 – *continued*

λ_{obs}	$F(\lambda)$	$I(\lambda)$	ID	λ_0	Mult
4408.60	8.33(−2)	8.52(−2)	[Fe II]	4406.38	
4412.07	1.01(−1)	1.03(−1)	[Fe II]	4409.85	V55e
4416.00	8.33(−2)	8.52(−2)	[Fe II]	4413.78	
4420.38	8.33(−2)	8.52(−2)	[Fe II]	4418.15	
4439.95	1.11(−1)	1.13(−1)	He I	4437.55	V50
4474.10	3.93	4.01	He I	4471.50	V14
4485.62	6.49(−2)	6.61(−2)	?	*	
4538.63	5.71(−2)	5.80(−2)	?	4535.96	
4543.46	5.05(−2)	5.13(−2)	?	4541.59	
4546.67	4.52(−2)	4.59(−2)	N III	4544.80	V12
4553.44	4.55(−2)	4.62(−2)	?	4550.76	
4565.18	2.06(−1)	2.09(−1)	Mg I]	4562.60	
4573.68	1.29(−1)	1.31(−1)	Mg I]	4571.10	
4589.44	5.49(−2)	5.56(−2)	?	4586.75	
4593.51	4.55(−2)	4.61(−2)	O II	4590.97	V15
4597.60	3.92(−2)	3.97(−2)	?	4594.90	V15
4598.72	1.99(−2)	2.02(−2)	O II	4596.18	V15
4609.66	4.23(−2)	4.29(−2)	[Fe III]	4607.13	3F
4633.28	3.86(−2)	3.91(−2)	N II	4630.54	V5
4641.96	3.07(−2)	3.11(−2)	O II	4638.49	V1
4644.60	6.30(−2)	6.37(−2)	N III	4640.64	V2
4652.34	5.38(−2)	5.44(−2)	O II	4649.13	V1
4654.05	5.06(−2)	5.12(−2)	O II	4650.84	V1
4654.68	7.01(−3)	7.08(−3)	?	4654.68	
4658.66	9.27(−2)	9.36(−2)	?	4655.92	
4661.01	1.63(−1)	1.65(−1)	[Fe III]	4658.10	3F
4664.28	7.91(−2)	8.00(−2)	O II	4661.63	V1
4685.79	3.89(−2)	3.92(−2)	?	4683.25	
4696.16	3.84(−2)	3.87(−2)	?	4693.31	
4704.42	4.37(−2)	4.40(−2)	[Fe III]	4701.62	3F
4714.07	3.03(−1)	3.05(−1)	[Ar IV]	4711.37	F1
4715.87	4.87(−1)	4.90(−1)	He I	4713.17	V12
4724.87	5.66(−2)	5.70(−2)	?	4722.83	
4742.99	2.05(−1)	2.06(−1)	[Ar IV]	4740.17	F1
4744.50	5.13(−2)	5.16(−2)	O II	4741.71	25
4757.83	5.77(−2)	5.80(−2)	[Fe III]	4754.83	3F
4760.61	3.71(−2)	3.73(−2)	Fe II?	4757.66	
4815.82	4.86(−2)	4.87(−2)	Si III	4813.20	
4818.07	5.85(−2)	5.86(−2)	S II	4815.45	V9
4820.77	7.88(−2)	7.90(−2)	?	4818.10	
4828.09	5.94(−2)	5.95(−2)	?	4825.61	
4833.25	6.59(−2)	6.60(−2)	?	4830.55	
4837.60	4.08(−2)	4.08(−2)	?	4834.70	
4842.50	5.94(−2)	5.94(−2)	?	4840.03	
4846.88	5.94(−2)	5.94(−2)	?	4844.15	
4864.06	1.00(+2)	1.00(+2)	H 4	4861.33	H4
4891.36	7.93(−2)	7.92(−2)	[Fe II]	4889.63	4F
4896.47	3.25(−2)	3.24(−2)	?	4893.75	
4905.43	5.59(−2)	5.57(−2)	[Fe IV]	4903.10	
4909.17	4.44(−2)	4.43(−2)	O II	4906.83	V28
4914.39	4.50(−2)	4.49(−2)	?	4914.84	
4917.57	4.50(−2)	4.49(−2)	?	4921.93	
4924.75	1.07	1.06	He I	4921.93	V48
4927.35	7.04(−2)	7.02(−2)	O II	4924.53	V28
4933.84	4.82(−2)	4.81(−2)	[O III]	4931.80	F1
4937.97	3.70(−2)	3.68(−2)	?	4934.52	
4943.12	7.05(−2)	7.02(−2)	O II	4941.07	V33
4965.36	1.70(+2)	1.69(+2)	[O III]	4958.91	F1
5013.46	5.12(+2)	5.08(+2)	[O III]	5006.84	F1
5525.05	3.57(−1)	3.46(−1)	[Cl III]	5517.66	F1
5545.02	4.41(−1)	4.28(−1)	[Cl III]	5537.60	F1
5760.62	1.31(−1)	1.26(−1)	[N II]	5754.60	F3
6142.57	5.97(−1)	5.67(−1)	?	6136.36	
6172.14	5.97(−1)	5.66(−1)	[Mn V]	6166.00	

Table 2 – *continued*

λ_{obs}	$F(\lambda)$	$I(\lambda)$	ID	λ_0	Mult
6204.09	2.57(−1)	2.44(−1)	O II	6197.92	
6237.22	2.16	2.04	[Ni III]	6231.09	
6260.46	1.65	1.56	[Fe II]	6254.30	
6301.05	1.56(+1)	1.48(+1)	[O I]	6300.34	F1
6312.81	1.73	1.64	[S III]	6312.10	F3
6467.49	2.05	1.93	C II	6461.95	
6499.73	2.05	1.93	?	6492.97	
6529.90	2.25	2.11	?WR	6516.12	
6543.22	2.04	1.91	?	6529.41	
6561.94	2.95	2.76	[N II]	6548.10	F1
6574.48	3.05(+2)	2.86(+2)	H3	6562.77	H3
6593.61	4.08	3.82	[N II]	6583.50	F1
6683.76	3.17	2.97	He I	6678.16	V46
6720.72	8.45	7.89	[S II]	6716.44	F2
6735.11	6.19	5.78	[S II]	6730.82	F2
7072.20	2.46	2.28	He I	7065.25	V10
7144.83	9.68	8.94	[Ar III]	7135.80	F1
7166.84	1.39	1.28	?	7159.07	
7178.54	3.61(−1)	3.34(−1)	[Ar IV]	7070.62	
7186.58	2.50(−1)	2.30(−1)	?	7186.58	
7293.51	5.73	5.27	He I	7281.35	V45
7333.56	1.92	1.77	[O II]	7318.92	F2
7344.32	1.68	1.55	[O II]	7329.67	F2

the temperature in zones where singly ionized species exist is predicted to be higher than T_e([O III]).

However, the contribution of recombination to the excitation of the [N II] λ5754 line (Rubin 1986), coupled with the potential presence of high-density inclusions in nebulae (Viegas & Clegg 1994), may cause deceptively high temperatures to be derived from the [N II] nebular to auroral line ratio, as well as from the corresponding [O II] λ3727/(λ7320 + λ7330) ratio. We have therefore estimated corrections to the [N II] temperatures of M 17, NGC 3576 and 30 Doradus, making use of the derived ORL N^{2+}/H^+ fractions presented later in Table 6 and equation (1) of Liu et al. (2000). The revised [N II] temperatures for these three nebulae are 7900, 8500 and 11 600 K, respectively; improved agreement with the corresponding [O III] temperatures of 8200, 8850 and 10 100 K is found in all cases. Given the inherent uncertainties, T_e(N II) values were not used in the abundance analysis that follows.

Regarding the derived electron densities, it is found that in four out of five nebulae the densities deduced from the [S II] λ6731/λ6716 ratio are in good agreement with those derived from the [O II] λ3729/λ3726 ratio (the spectral resolution was not adequate to allow the determination of the [O II] doublet ratio in M 17), but are lower than the values given by the [Ar IV] and [Cl III] diagnostics. This can be seen especially in LMC N11B and SMC N66 where the [O II] and [S II] doublet ratios approach the low-density limit, and certainly imply N_e an order of magnitude less than from the doubly ionized species (Table 3). This behaviour is consistent with the presence of strong density variations in the nebulae, so that diagnostic line ratios from lines with higher critical densities[1] yield higher derived nebular electron densities (see Rubin 1989; Liu 2001a).

[1] For [Cl III] λλ5517, 5537, $N_{cr} = 6400$ and 34 000 cm^{-3}; for [Ar IV] λλ4711, 4740, $N_{cr} = 14\,000$ and 130 000 cm^{-3}; for [O II] λλ3726, 3729, $N_{cr} = 4300$ and 1300 cm^{-3}; and for [S II] λλ6716, 6730, $N_{cr} = 1200$ and 3300 cm^{-3} respectively; the quoted values are for an electron temperature of 10 000 K.

Table 3. Plasma diagnostics.

Diagnostic ratio	M 17	NGC 3576	30 Doradus	LMC N11B	SMC N66
			T_e (K)		
[O III] (λ4959+λ5007)/λ4363	8200	8850	10100	9400	12400
[N II] (λ6548+λ6584)/λ5754	9100	9000	12275	9250	14825
	7900[a]	8500[a]	11600[a]	*	*
[S II] λ4068/(λ6717+λ6730)	8850	7900	7500	6950	11050
BJ/H 11	7700	8070	*	*	*
T_0	7840	8300	*	*	*
t^2	0.011	0.017	*	*	*
			N_e (cm^{-3})		
[Ar IV] λ4740/λ4711	1500	1700	1800	*	$\lesssim$100
[Cl III] λ5537/λ5517	1050	2700	480	1700	3700
[S II] λ6731/λ6716	600	1350	390	80	60
[O II] λ3729/λ3726	*	1300	370	110	50

[a][N II] temperatures after correction for recombination excitation contributions.

4 IONIC AND TOTAL ELEMENTAL ABUNDANCES FROM CELs

We used the statistical equilibrium code EQUIB to derive ionic abundances from nebular CELs. The ionic abundances deduced are presented in Table 4. For each nebula, the electron temperature derived from the [O III] nebular to auroral line ratio was adopted for all ionic species, following the discussion detailed in the previous section. Regarding the choice of electron densities, we adopted the mean of the values deduced from the [O II] and [S II] doublet ratios in order to derive abundances of singly ionized species, while the mean electron densities from the [Ar IV] and [Cl III] ratios were used to derive abundances for doubly and triply ionized species.

Total abundances from CELs have been derived adopting the ICF scheme of Kingsburgh & Barlow (1994), apart from Cl which was not discussed by those authors. For that element and in the cases of M 17, 30 Doradus and SMC N66, the prescription of Liu et al. (2000) was used, according to which $Cl/H = (S/S^{2+}) \times Cl^{2+}/H^+$, based on the similarities of the ionization potentials of chlorine ionic stages to those of sulphur ionic stages. On the other hand, for NGC

Table 4. Ionic and elemental abundances for helium relative to hydrogen, derived from ORLs, and those for heavy elements, derived from CELs.[a]

λ_0 (Å)		M 17	NGC 3576	30 Doradus	LMC N11B	SMC N66
4471	He^+/H^+	0.0955(1)	0.0949(1)	0.0874(1)	0.0856(1)	0.0791(1)
5876	He^+/H^+	0.0959(4)	0.0926(4)	0.0910(3)	0.1022(4)	0.1006(4)
6678	He^+/H^+	0.0909(1)	0.0879(1)	0.0926(1)	0.0906(1)	0.0756(1)
Avg.	He/H	0.0950	0.0922	0.0906	0.0975	0.0928
3727	O^+/H^+	9.28(−5)	1.10(−4)	4.13(−5)	1.12(−4)	3.35(−5)
7320+7330	–	1.18(−4):	2.06(−4):	5.77(−5):	3.79(−4):	8.77(−6):
4931	O^{2+}/H^+	2.23(−4):	3.31(−4):	*	2.36(−4):	6.30(−5):
4959	–	2.66(−4)	2.21(−4)	1.76(−4)	1.47(−4)	9.41(−5)
	icf(O)	1.00	1.00	1.00	1.00	1.00
	O/H	3.59(−4)	3.31(−4)	2.17(−4)	2.59(−4)	1.28(−4)
6548+6584	N^+/H^+	8.14(−6)	1.17(−5)	1.48(−6)	3.66(−6)	5.37(−7)
	icf(N)	3.87	3.01	5.25	2.31	3.82
	N/H	3.15(−5)	3.52(−5)	7.77(−6)	8.45(−6)	2.05(−6)
3868+3967	Ne^{2+}/H^+	7.17(−5)	3.46(−5)	3.71(−5)	2.40(−5)	1.72(−5)
	icf(Ne)	1.39	1.50	1.23	1.76	1.36
	Ne/H	9.97(−5)	5.19(−5)	4.56(−5)	4.22(−5)	2.34(−5)
7135	Ar^{2+}/H^+	1.48(−6)	1.70(−6)	1.11(−6)	1.12(−6)	4.71(−7)
4711+4740	Ar^{3+}/H^+	2.72(−8)	2.15(−8)	3.39(−8)	2.27(−8)	3.16(−8)
	icf(Ar)	1.35	1.50	1.24	1.76	1.35
	Ar/H	2.03(−6)	2.58(−6)	1.42(−6)	2.01(−6)	6.79(−7)
4069	S^+/H^+	5.79(−7):	7.50(−7):	2.53(−7):	8.82(−7):	2.60(−7):
6716+6730	–	3.60(−7)	6.20(−7)	2.80(−7)	7.32(−7)	2.59(−7)
6312	S^{2+}/H^+	8.05(−6)	*	4.28(−6)	*	1.66(−6)
	icf(S)	1.19	*	1.29	*	1.19
	S/H	1.00(−5)	6.57(−7)	5.88(−6)	4.98(−6)	2.28(−6)
5517	Cl^{2+}/H^+	1.07(−7)	9.95(−8)	5.14(−8)	7.69(−8)	2.63(−8)
	icf(Cl)	1.24	1.52	1.37	1.79	1.37
	Cl/H	1.33(−7)	1.51(−7)	7.04(−8)	1.38(−7)	3.60(−8)

[a]Numbers followed by ':' have not been used at any point in the analysis. The numbers in parentheses following the He^+/H^+ abundances are the weighting factors used for the derivation of the average He^+/H^+ abundance.

3576 and LMC N11B, for which the listed S abundances are lower limits, we adopted $Cl/H = (Ar/Ar^{2+}) \times Cl^{2+}/H^{+}$. The total oxygen abundance was adopted to be the sum of singly and doubly ionized oxygen abundances. No significant amounts of O^{3+} are expected, because no He II recombination lines are seen.

5 IONIC ABUNDANCES FROM ORLs

Because ionic abundances relative to H^{+} derived from intensity ratios of heavy-element ORLs relative to a hydrogen recombination line depend only weakly on the adopted temperature, and are essentially independent of N_e, for each nebula the [O III] temperature was adopted for the calculations. The He abundances derived from He I recombination lines are given in Table 4. Case A recombination was assumed for the triplet lines λ4471, λ5876 and Case B for the singlet λ6678 line. The effective recombination coefficients are from Brocklehurst (1972). For the λ4471 line, the effective coefficient given by Brocklehurst (1972) differs by only 1.4 per cent from the calculations of Smits (1996). The differences between the two calculations are even smaller for the other two lines. Contributions to the observed fluxes by collisional excitation from the He^0 2s ^{3}S metastable level by electron impacts were corrected for using the formulae derived by Kingdon & Ferland (1995a).

In the following subsections we present C, N and O ionic abundances derived from ORLs.

5.1 C^{2+}/H^{+} and N^{2+}/H^{+}

The case-insensitive C II λ4267 (4f–3d) line has been detected from all nebulae except SMC N66 and used to derive the C^{2+}/H^{+} abundance ratios presented in Table 5; an upper limit only has been estimated for SMC N66. The doublet from multiplet V4 (λ3920) has also been detected from NGC 3576, but not used for abundance determinations as its upper levels are directly connected to the C^{+} $2p^2\,P^o$ ground term, and the doublet is therefore potentially affected by optical depth effects.

Regarding the N^{2+}/H^{+} ORL abundance ratios, these have been derived for M 17 and NGC 3576 and are presented in Table 6; lines from the N II 3s–3p V3 and V5 multiplets have been detected and Case B recombination has been assumed. It is estimated that under Case A the abundance ratios deduced from the V5 lines would be several times higher, while V3 results would be larger by only about 20 per cent. Longer exposure times would be required to detect the weaker case-insensitive lines from the 3d–4f group. N II ORLs have not been unambiguously detected from any of the Magellanic Cloud H II regions; the strongest predicted multiplet V3 (λ5680) is probably present in 30 Doradus, but the resolution of our spectra is too low (FWHM 11 Å) at this wavelength to allow us to be conclusive. In the spectrum of that nebula, the strongest N II V5 multiplet line, at 4630 Å, is marginally detected; an upper limit to the N^{2+}/H^{+} fraction of 5.48×10^{-5} was derived from it. From Table 6 we adopt N^{2+}/H^{+} fractions of 3.53×10^{-4} and 2.70×10^{-4} for M 17 and NGC 3576, respectively.

Table 5. Ionic carbon abundances from optical recombination lines.

	M 17	NGC 3576	30 Dor	LMC N11B	SMC N66
$I(\lambda 4267)$	0.482	0.312	0.0919	0.196	$\lesssim$0.0419
$\mathbf{10^4 \times C^{2+}/H^{+}}$	**4.35**	**2.87**	**0.882**	**1.82**	$\mathbf{\lesssim 0.433}$

5.2 O^{2+}/H^{+}

To our knowledge, this is the first time that O II ORLs arising from Magellanic Cloud H II regions have been recorded. We have detected transitions from 3s–3p, as well as 3p–3d and 3d–4f configurations. In Table 7 we present a comparison between the observed and predicted intensities of O II lines relative to the strongest expected line within each multiplet. The numbers in brackets are the formal absolute errors to the intrinsic intensities derived from the line-fitting method only; they do not include any possible systematic errors arising, for example, from the flux calibration of our spectra. As with our extensive O II optical recombination-line survey of planetary nebulae (Tsamis et al. 2003b), it is assumed that *LS* coupling holds for the 3s–3p transitions, while intermediate coupling is assumed for those between 3p–3d and 3d–4f states (Liu et al. 1995a). Table 7 is important both for checking whether observation agrees with theory and in excluding some lines from further consideration when blending or misidentification are suspected.

5.2.1 Relative intensities of O II ORLs

In contrast to our results from a comparison of PN O II relative line intensities (Tsamis et al. 2003b), there is clear evidence that several transitions are stronger than expected in all five H II regions studied (Table 7). The effect is especially pronounced amongst the lines of O II multiplet V1; those of multiplet V10, however, are in better agreement with theory even though their formal measurement errors are somewhat larger due to partial blending with the [S II] λλ4068, 4076 doublet. A similar situation has been reported by Esteban et al. (1999) from their echelle observations of the Lagoon Nebula (M 8). Esteban et al. (1998), however, found quite good agreement between O II multiplet V1 lines from the Orion Nebula, a result supported by our examination of the relative intensities of the same transitions

Table 6. Recombination-line N^{2+}/H^{+} abundances.

λ_0 (Å)	Mult.	I_{obs}	$\frac{N^{2+}}{H^{+}}$ (10^{-4})	I_{obs}	$\frac{N^{2+}}{H^{+}}$ (10^{-4})	I_{obs}	$\frac{N^{2+}}{H^{+}}$ (10^{-4})
		M 17		NGC 3576		30 Doradus	
V3 $3s^3P^o$–$3p^3D$							
5666.63	V3	.0569	4.35	.0358	2.80	*	*
5676.02	V3	.0170	2.93	.0159	2.72	*	*
5679.56	V3	.0544	2.23	.0667	2.75	*	*
V5 $3s^3P^o$–$3p^3P$							
4630.54	V5	.0602	4.99	.0309	2.56	.0066	.548
V20 $3p^3D$–$3d^3D^o$							
4803.29	V20	.0304	4.52	*	*	*	*
Sum		**.219**	**3.53**	**.149**	**2.70**	*	**.548**

Table 7. Comparison of the observed and predicted relative intensities of O II ORLs.

λ_0 (Å)	Mult	Term$_l$–Term$_u$	g$_l$–g$_u$	$I_{\rm pred}$	$I_{\rm obs}$	$I_{\rm obs}/I_{\rm pred}$
			M 17			
(3s–3p)						
4638.86	V1	3s 4P–3p 4D*	2–4	0.21	0.77[.12]	3.7[0.6]
4641.81	V1	3s 4P–3p 4D*	4–6	0.53	1.11[.16]	2.1[0.3]
4649.13	V1	3s 4P–3p 4D*	6–8	1.00	1.00[.10]	1.0[0.1]
4650.84	V1	3s 4P–3p 4D*	2–2	0.21	0.63[.11]	3.0[0.5]
4661.63	V1	3s 4P–3p 4D*	4–4	0.27	0.76[.11]	2.8[0.4]
4676.24	V1	3s 4P–3p 4D*	6–6	0.22	0.46[.10]	2.1[0.5]
4317.14	V2	3s 4P–3p 4P*	2–4	0.44	1.04[.32]	2.6[0.8]
4319.63	V2	3s 4P–3p 4P*	4–6	0.43	0.31[.23]	0.7[0.5]
4345.56	V2	3s 4P–3p 4P*	4–2	0.40	0.63[.20]	1.5[0.5]
4349.43	V2	3s 4P–3p 4P*	6–6	1.00	1.00[.10]	1.0[0.1]
			NGC 3576			
(3s–3p)						
4638.86	V1	3s 4P–3p 4D*	2–4	0.21	0.55[.11]	2.6[0.5]
4641.81	V1	3s 4P–3p 4D*	4–6	0.53	0.95[.16]	1.8[0.3]
4649.13	V1	3s 4P–3p 4D*	6–8	1.00	1.00[.10]	1.0[0.1]
4650.84	V1	3s 4P–3p 4D*	2–2	0.21	0.60[.11]	2.9[0.5]
4661.63	V1	3s 4P–3p 4D*	4–4	0.27	0.99[.16]	3.7[0.6]
4676.24	V1	3s 4P–3p 4D*	6–6	0.22	0.60[.16]	2.7[0.7]
(3p–3d)						
4069.89	V10	3p 4D∗ –3d 4F	4–6	0.74	1.40[.20]	1.9[0.3]
4072.16	V10	3p 4D∗ –3d 4F	6–8	0.69	1.20[.82]	1.7[1.2]
4075.86	V10	3p 4D∗ –3d 4F	8–10	1.00	1.00[.10]	1.0[0.1]
4085.11	V10	3p 4D∗ –3d 4F	6–6	0.13	0.17[.10]	1.3[0.8]
(3d–4f)						
4087.15	V48c	3d 4F–4f G3*	4–6	0.27	1.30[.48]	4.8[1.8]
4089.29	V48a	3d 4F–4f G5*	10–12	1.00	1.00[.10]	1.0[0.1]
4275.55	V67a	3d 4D–4f F4*	8–10	1.20	4.18[1.1]	3.5[0.9]
4357.25	V63a	3d 4D–4f D3*	6–8	0.05	2.36[.85]	47.[17.]
4609.44	V92a	3d 2D–4f F4*	6–8	0.14	1.69[.64]	12.[5.0]
			30 Doradus			
(3s–3p)						
4638.86	V1	3s 4P–3p 4D*	2–4	0.21	1.00[.15]	4.8[0.7]
4641.81	V1	3s 4P–3p 4D*	4–6	0.53	1.33[.18]	2.5[0.3]
4649.13	V1	3s 4P–3p 4D*	6–8	1.00	1.00[.10]	1.0[0.1]
4650.84	V1	3s 4P–3p 4D*	2–2	0.21	1.00[.19]	4.8[0.9]
4661.63	V1	3s 4P–3p 4D*	4–4	0.27	0.88[.12]	3.3[0.4]
4673.73	V1	3s 4P–3p 4D*	4–2	0.04	0.19[.03]	4.8[0.8]
4676.24	V1	3s 4P–3p 4D*	6–6	0.22	0.35[.05]	1.6[0.2]
4317.14	V2	3s 4P–3p 4P*	2–4	1.00	1.00[.10]	1.0[0.1]
4319.63	V2	3s 4P–3p 4P*	4–6	0.98	1.06[.12]	1.1[0.1]
(3p–3d)						
4069.89	V10	3p 4D∗ –3d 4F	4–6	1.00	1.00[.10]	1.0[0.1]
4072.16	V10	3p 4D∗ –3d 4F	6–8	0.93	0.51[.09]	0.6[0.1]
4078.84	V10	3p 4D∗ –3d 4F	4–4	0.14	0.24[.05]	1.7[0.4]
4085.11	V10	3p 4D∗ –3d 4F	6–6	0.17	0.19[.04]	1.1[0.2]
(3d–4f)						
4083.90	V48b	3d 4F–4f G4*	6–8	0.29	0.51[.31]	1.8[1.1]
4087.15	V48c	3d 4F–4f G3*	4–6	0.27	0.88[.23]	3.3[0.9]
4089.29	V48a	3d 4F–4f G5*	10–12	1.00	1.00[.13]	1.0[0.1]
4275.55	V67a	3d 4D–4f F4*	8–10	1.33	3.73[.71]	2.8[0.5]
4288.82	V53c	3d 4P–4f D1*	2–4	0.83	11.9[2.6]	14.[3.0]
4303.83	V53a	3d 4P–4f D3*	6–8	0.50	2.47[.44]	4.9[0.9]
4313.44	V78a	3d 2F–4f F4*	8–10	0.61	2.06[.68]	3.4[1.1]
4315.69	V63c	3d 4D–4f D1*	6–4	0.11	1.82[.67]	17.[6.0]
4609.44	V92a	3d 2D–4f F4*	6–8	0.57	1.00[.24]	2.0[0.4]
			LMC N11B			
(3s–3p)						
4638.86	V1	3s 4P–3p 4D*	2–4	0.21	1.54[.15]	7.3 [0.7]
4641.81	V1	3s 4P–3p 4D*	4–6	0.53	0.70[.18]	1.3 [0.3]
4649.13	V1	3s 4P–3p 4D*	6–8	1.00	1.00[.10]	1.0 [0.1]
4650.84	V1	3s 4P–3p 4D*	2–2	0.21	0.83[.19]	4.0 [0.9]
4661.63	V1	3s 4P–3p 4D*	4–4	0.27	0.84[.12]	3.1 [0.4]

Table 7 – *continued*

λ_0 (Å)	Mult	Term$_l$–Term$_u$	g$_l$–g$_u$	$I_{\rm pred}$	$I_{\rm obs}$	$I_{\rm obs}/I_{\rm pred}$
4673.73	V1	3s 4P–3p 4D*	4–2	0.04	0.41[.03]	10.[1.0]
4676.24	V1	3s 4P–3p 4D*	6–6	0.22	0.36[.05]	1.6 [0.2]
			SMC N66			
(3s–3p)						
4638.86	V1	3s 4P–3p 4D*	2–4	0.21	0.57[.15]	2.7[0.7]
4649.13	V1	3s 4P–3p 4D*	6–8	1.00	1.00[.10]	1.0[0.1]
4650.84	V1	3s 4P–3p 4D*	2–2	0.21	0.94[.19]	4.5[0.9]
4661.63	V1	3s 4P–3p 4D*	4–4	0.27	1.47[.32]	5.4[1.2]

using the recent Orion line atlas by Baldwin et al. (2000), which has better spectral resolution than the data used by the former authors. Our observations show that for all five H II regions the λ4638.86 (J = 1/2–3/2) and λ4650.84 (J = 1/2–1/2) V1 transitions are enhanced from each nebula: by a factor ranging from ∼2.8–7.3 for the five objects under study; for Orion this factor is only ∼1.4 for both lines, but less for the other V1 transitions. The λ4661.63 (J = 3/2–3/2) line is also abnormally strong compared to theory.

One possible explanation for this behaviour involves the breakdown of thermal equilibrium among the fine-structure levels of the parent $^3P_{0,1,2}$ ground term of recombining O^{2+}. Our analysis of the O II 3s–3p transitions employed term-averaged effective recombination coefficients from Storey (1994) which were calculated assuming that the O II 3s and 3p levels are well described by *LS* coupling. When this is the case, the population distribution among the O^{2+} $^3P_{0,1,2}$ levels has no effect on the recombination rate to these levels. If, however, there is a breakdown of *LS* coupling so that the recombination rate coefficients from the individual ^3P_J levels differ, then the total recombination coefficient to a particular O II 3p state becomes a function of the population distribution among the ^3P_J levels. There are no published results for the O II recombination coefficients that take account of such effects but we have made a trial calculation of the inverse process of photoionization from the 3p $^4D_{7/2}$ level, the upper state of the λ4649.13 transition. This calculation shows that the direct recombination to this level comes overwhelmingly from the O^{2+} $^3P_2$ level. Recombination from the $^3P_{0,1}$ levels is negligible. Therefore, if the population of the O^{2+} $^3P_2$ level falls below that expected in thermal equilibrium the true recombination rate to the 3p $^4D_{7/2}$ level will be less than that predicted by the *LS* coupling results of Storey (1994) and the λ4649.13 line will be observed to be weaker than is predicted by the *LS* coupling theory. The relative populations of the O^{2+} $^3P_{0,1,2}$ levels will depart from thermal equilibrium if the electron density of the nebula is lower than the critical densities of one or both of the $^3P_{1,2}$ levels (∼500 and 3500 cm^{-3}). The mean electron density derived from various diagnostics for the objects under study here is in all cases lower than 2000 cm^{-3}, while for the three Magellanic Cloud H II regions that show the greatest deviations from the predicted *LS* coupling relative intensities for O II V1 multiplet transitions,[2] it is lower than 1000 cm^{-3} (Table 3); this is in contrast to M 42, for which Esteban et al. (1998) find $N_e \simeq$ 5000 cm^{-3}. Thus, it seems that within multiplet V1 the strongest expected line, namely λ4649.13 (J = 5/2–7/2), is weakened at the expense of transitions between levels of lower J. This argument seems to be supported by our analysis of O II ORLs originating from planetary nebulae (Liu et al. 1995a, 2000, 2001b; Tsamis 2002; Tsamis et al. 2003b). For example, the observed relative intensities of V1 lines from the dense planetary nebulae IC 4191 and NGC 5315 are in perfect agreement with theory (Tsamis et al. 2003b); the derived mean electron densities of these objects are 10 700 and 14 100 cm^{-3}, respectively. The opposite is true in the case of the PN NGC 3132 ($N_e \simeq$ 600 cm^{-3}), where the V1 lines display abnormal ratios (Tsamis et al. 2003b), just as they do for the H II regions considered here. We will return to this issue in a future paper (Tsamis et al. 2003b), by combining our H II region ORL data set from this paper with the PN ORL data set of Tsamis et al. (2003b) in order to plot the relative intensities of O II V1 multiplet components as a function of nebular electron density.

If the above interpretation is correct, the total observed intensity of the whole multiplet should not be affected and can be used to derive a reliable ORL O^{2+}/H^+ abundance. A similar effect may dictate the relative intensities of lines from the 3d–4f group, weakening the λ4089 transition (Liu 2002b).

A major point to be deduced from this analysis is that the observed relative intensities of O II recombination lines point towards their origin in low-density gas (<3500 cm^{-3}), similar to that emitting the [O III] and other CELs.

5.2.2 *Continuum observations and scattered light*

An issue, which had to be addressed in the course of this analysis, is the potential influence of dust-scattered stellar light on the intensities of weak nebular emission features such as the O II ORLs of interest. Unlike PNe, where the size of the emitting region results in relatively small dust columns, the situation is different in H II regions whose large volumes contain much larger dust columns. The dust effectively scatters light from the nebula's illuminating stars, which then makes up a major fraction of the observed continuum at UV and optical wavelengths. It is thus possible that emission or absorption features in the spectra of the exciting stars in an H II region may contaminate the nebular emission spectrum. Peimbert et al. (1993) dealt with this problem in an analysis of the M 42 and M 17 H II regions. They employed previously published medium resolution (5–7 Å) spectroscopic data in order to derive ORL O^{2+}/H^+ abundances; their resolution, however, was not adequate to allow for the effect of blending of O II ORLs with other lines, e.g. [Fe II], N III and C III, so they resorted to older photographic line intensities in order to estimate the necessary corrections. Our CCD spectrophotometry is of significantly higher resolution (1, 1.5 and 2 Å for the coverage of O II ORLs) and our line intensities are consistently corrected for blends with other nebular emission lines.

In order to investigate the potential effect of dust-scattered stellar light on the nebular line fluxes, we have measured the continuum emission at 4089 and 4650 Å, which coincide with the strongest 3d–4f O II transition at 4089.3 Å, and O II multiplet V1 ORLs,

[2] Large deviations are still present even if corrections are made for O II absorption features in the nebular continuum component, attributable to dust-scattered starlight (see Section 5.2.2).

Table 8. Continuum emission and scattered light, expressed as log $I^c(\lambda)/I(H\beta)$.

	M 17		NGC 3576		30 Doradus		LMC N11B		SMC N66	
	$I^c(\lambda)$	$I^c(\lambda)_d$	$I^c(\lambda)$	$I^c(\lambda)_d$	$I^c(\lambda)$	$I^c(\lambda)_d$	$I^c(\lambda)$	$I^c(\lambda)_d$	$I^c(\lambda)$	$I^c(\lambda)_d$
λ4089	−2.402	−2.508	−2.218	−2.279	−2.433	−2.564	−2.063	−2.135	−2.103	−2.168
λ4650	−2.645	−2.806	−2.435	−2.522	−2.624	−2.797	−2.278	−2.357	−2.214	−2.283

Table 9. Estimated equivalent widths (in units of m Å).

	30 Doradus		LMC N11B	
	EW_{em}	$EW_{abs(neb)}$	EW_{em}	$EW_{abs(neb)}$
λ4072	185	107	*	*
λ4089	57	87	151	98
λ4640	637	37	286	167
λ4650	540	185	264	298
λ4661	238	40	121	78

respectively. In Table 8 the continuum intensity, I^c (λ), and the scattered light contribution, I^c $(\lambda)_d$, to the observed continuum are presented. The observed continuum is mainly due to two components – the nebular atomic continua and dust-scattered starlight – so that

$$I^c(\lambda) = I^c(\lambda)_a + I^c(\lambda)_d,$$

where I^c $(\lambda)_a$ represents the sum of the H I and He I atomic continua calculated using emissivities from Storey & Hummer (1995) and Brown & Mathews (1970), respectively; the T_e, N_e and He^+/H^+ for each object were taken into account. We find that for M 17, dust-scattered light accounts for 78 and 69 per cent of the observed continuum at 4089 and 4650 Å, respectively; for NGC 3576 these values are 87 and 82 per cent; for 30 Doradus the corresponding values are 74 and 67 per cent; for LMC N11B they are 85 and 83 per cent; finally, for SMC N66 they are 86 and 85 per cent, respectively (sky-subtraction has not been carried out; the sky contribution was estimated to be negligible for these dark-of-Moon conditions).[3]

In Table 9 we present estimated equivalent widths, $EW_{abs(neb)}$, for stellar lines in absorption (in mÅ) in the observed nebular continuum, given by

$$EW_{abs(neb)} = EW_{abs(stellar)} I^c(\lambda)_d / I^c(\lambda), \quad (1)$$

with the continuum intensity values being those given in Table 8. This analysis pertains to the stellar content of 30 Doradus in the following way. According to (Walborn & Blades, 1997 WB97), the visually brightest stars in the 30 Doradus association are B-type supergiants, along with the Of-type star R139 (=Parker 952). Therefore, we will assume that such stellar spectra dominate the observed dust-scattered light. We have singled out seven stars which are the brightest in the central ∼1 arcmin^2 of the cluster (excluding the compact core R136): R137 = P548 [B0.7–1.5 I, V = 12.14]; R138 [A0Ia, V = 11.87]; R139[4] = P952 [WNL + Of, V = 11.94]; R140 = P877, 880 [WN + WC, V = 12.22, 12.79]; R141 = P1253 [BN0.5 Ia, V = 12.57]; R142 = P987 [B0.5–0.7 I, V = 11.91]; and P767 [O3 If*, V = 12.87].

We have high-resolution spectrograms (at 0.9 Å per pixel) of R139 (Fig. 2) and R140 (Fig. 3), because they fell on our slit; the remaining five stars were positioned on either side of it. It is assumed that the spectra of R137 and R142 are similar to that of Parker 3157 (V = 12.47; Parker et al. 1992)[5] a supergiant belonging to the LMC LH10 (N11) association, whose spectrogram (at 0.9 Å per pixel) was extracted from our LMC N11B frames (Fig. 4). High-resolution spectra of R141 and P767 can be found in WB97; we do not have a spectrum of R138, but we can safely assume that it is featureless at the wavelengths of interest judging from its spectral type.

The O II spectrum reaches a sharp maximum in absorption in stars of early-B spectral type (e.g. Walborn & Fitzpatrick 1990), thus the very existence of B-type supergiants in nebulae complicates the analysis of nebular O II ORLs. It is therefore recommended that fields of view relatively clear of such stars are chosen for future weak-emission line analyses of H II regions. The stellar absorption and/or emission features that are of relevance to this analysis are: Si IV + O II λ4089, N III + O II λλ4638, 4640, C III + O II λ4650 and O II λ4661.

Values of $EW_{abs(stellar)}$ were estimated at wavelengths of interest on the stellar spectrograms mentioned above and subsequently averaged, weighted according to the brightness ratios of the seven illuminating stars in the blue wavelength region, i.e. 5.6 : 6.3 : 4.3 : 6.8 : 3.2 : 9.8 : 1.0 (for R137 : R138 : R139 : R140 : R141 : R142: P767). We have assumed a total-to-selective extinction ratio of $R_B = A_B/E(B-V) = 5$ (Hill et al. 1993) and adopted apparent magnitudes and $(B-V)$, $E(B-V)$ values from Parker (1993). We were then able to compute the $EW_{abs(neb)}$ values in Table 9 using equation (1). To correct the observations, we should add these to the observed EW_{em} values.

Considering LMC N11B, we found the early-B supergiant Parker 3157, with its extremely rich O II absorption line spectrum, directly in the field of view of the spectrograph slit (Fig. 4). Absorption lines in the scattered light from this star are responsible for a significant drop in the intensity of the observed continuum in the region of the λλ4638, 4640, 4649, 4650 and λ4661 lines of multiplet V1. In contrast to 30 Doradus however, the dust-scattered light in N11B does not contain any obvious contribution from Of- and WR-type stars equivalent to, for example, R139 or R140 – no Wolf–Rayet stars are listed in the census of N11B by Parker et al. (1992) – whose *emission* lines in the λ4650 region can partly compensate for absorption lines due to early-B supergiants, resulting in a fairly level continuum at those wavelengths for the former nebula. Therefore, together with the supergiant P3157, we will assume that the

[3] A typical dark-of-Moon sky brightness at B (4400 Å) is $22^m.8$ per arcsec^2 corresponding to 4.73×10^{-18} erg s^{-1} cm^{-2} Å^{-1} arcsec^{-2} when $B = 0$ is 6.24×10^{-9} erg s^{-1} cm^{-2} Å^{-1}; thus, for 30 Doradus, for example, the sky contribution to the observed continuum at λ4650 is ∼0.082 per cent only.

[4] Whereas Moffat et al. (1987) and Moffat (1989) classify R139 as a WNL/Of-type binary system, WB97 classify it as an O7 Iafp-type single star. Our spectrum shown in Fig. 2 is of higher resolution than that of WB97 and supports a classification of O6.5 Ib(f) + WNL for R139.

[5] Parker et al. (1992) classify P3157 as spectral type BC1 Ia. However, our analysis of its spectrum (Fig. 4) does not reveal the presence of any C III lines at 4650 Å. The absorption features at that wavelength can be fitted purely by O II V1 multiplet lines. We therefore suggest a revised spectral type of B1 Ia for P3157.

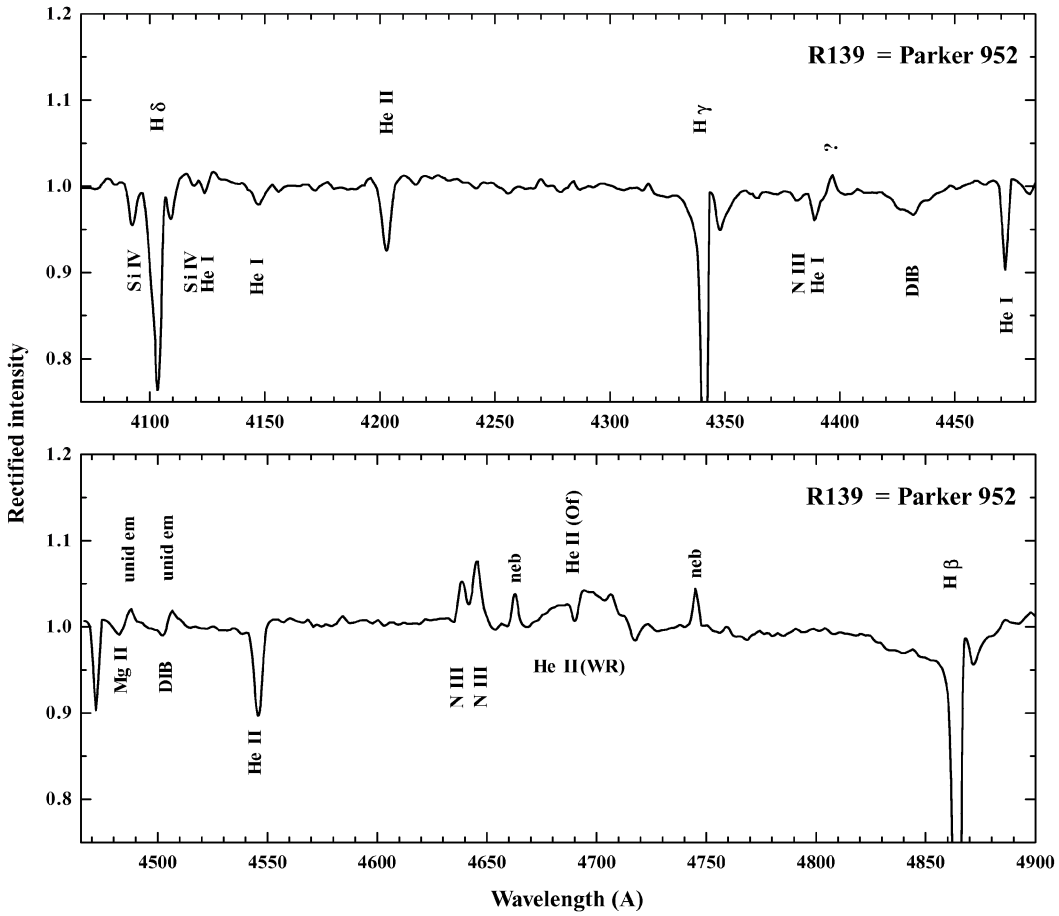

Figure 2. Rectified blue–violet spectrogram of the O6.5 Ib(f) + WNL multiple star R139 (=Parker 952) in 30 Doradus. The identified features are: Hδ λ4102, Hγ λ4340, Hβ λ4861; He I $\lambda\lambda$4121, 4144, 4387, 4471; He II $\lambda\lambda$4200, 4541, 4686 (broad WR emission + narrow absorption); N III λ4379, ($\lambda\lambda$4638, 4640+4641 emission); Si IV $\lambda\lambda$4089, 4116; Mg II λ4481; the diffuse interstellar bands at $\lambda\lambda$4430, 4502 and the unidentified emission lines at $\lambda\lambda$4485, 4503. See text for more details.

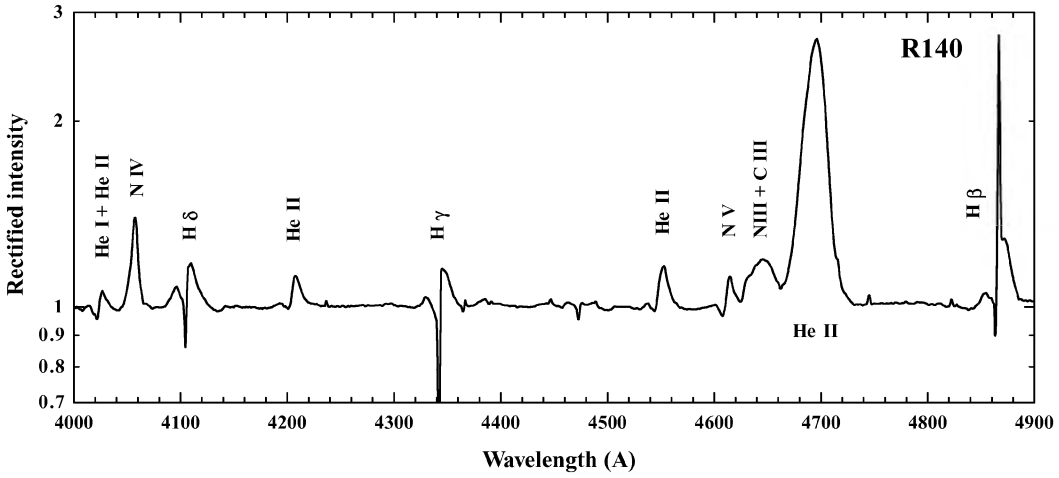

Figure 3. Rectified log-intensity, blue–violet spectrogram of the WN6(h) component of the multiple star R140 in 30 Doradus. The identified features are: Hδ λ4102, Hγ λ4340, Hβ λ4861, He I λ4026; He II $\lambda\lambda$4026, 4200, 4541, 4686; N III $\lambda\lambda$4638 + 4640 + 4641; N IV λ4058; N V $\lambda\lambda$4603, 4619. See text for more details.

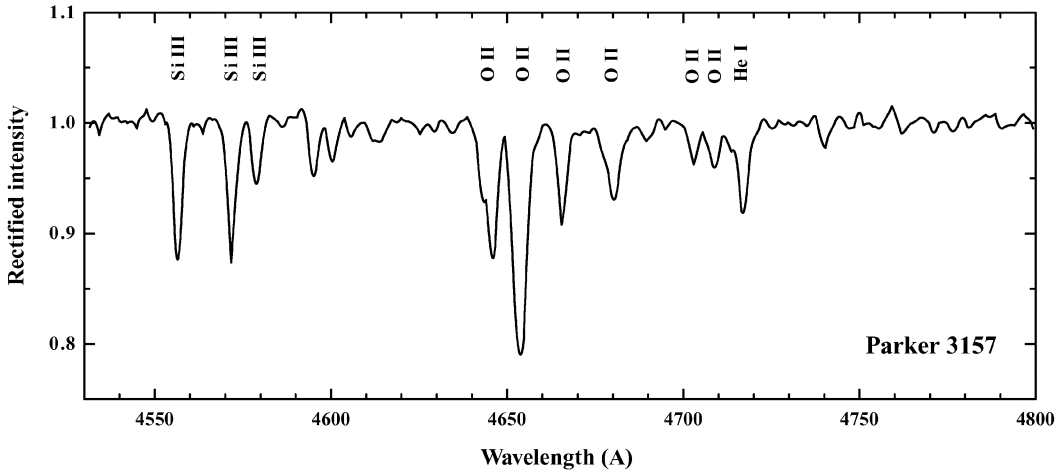

Figure 4. Rectified, blue spectrogram of the B1 Ia-type supergiant Parker 3157 in LMC N11B which has a full complement of O II V1 multiplet absorption lines. See text for more details.

observed continuum in N11B is dominated by the scattered light of six other stars, which are visually the brightest amongst those studied by Parker et al. (1992). These are: P3209 [O3 III(f*), $V = 12.66$]; P3252 [B2 II, $V = 11.35$]; P3271 [B1 II, $V = 12.99$]; P3070 [O6 V, $V = 12.75$]; P3223 [O8.5 IV, $V = 12.95$]; and P3120 [O5.5 V ((f*)), $V = 12.80$]. High-resolution rectified spectrograms for these stars have been presented by Parker et al. and have been used to estimate mean $EW_{\rm abs(stellar)}$ values. More accurate measurements were possible for P3157 for which we have a digital spectrogram. A cross-comparison between our digital spectrogram and those presented by Parker et al. (1992), including P3157, shows agreement, pointing towards a reliable estimate of the *EW* values.

In Table 10 we present the measured intensities and the derived abundances from O II ORLs for all five H II regions, *before any correction for scattered light contamination*. Along with values obtained from individual transitions, abundances derived from total multiplet intensities are also listed (in bold face) and are discussed in more detail below for each object. In the context of this discussion, revised abundance ratios are then presented, incorporating corrections for the effects of the scattered stellar continua on the measured nebular emission line intensities wherever possible.

M 17: The two triplet 3s–3p multiplets V1 and V2 are detected, yielding similar results. The mean O^{2+}/H^+ abundance ratio is 5.68×10^{-4}. Peimbert et al. (1993) have derived a very similar value of 4.85×10^{-4} using multiplets V1 and V5 after correcting the line intensities for underlying absorption due to dust-scattered stellar light. We have not taken into account such an effect for this nebula, because the corrections of Peimbert et al. amount to only 14 per cent for multiplet V1, that is affected the most. A comparison with the forbidden-line abundance from Table 3 yields an ORL/CEL abundance ratio of 2.1 for O^{2+} (Section 7.1, Table 12).

NGC 3576: Multiplets V1 and V10 yield consistent results; lines from the 3d–4f group display abnormal intensity ratios. It is likely that underlying absorption affects the λ4089 transition. We do not attempt any corrections and adopt for the ORL O^{2+}/H^+ ratio the mean of the V1 and V10 results, i.e. 3.70×10^{-4}. The ORL/CEL ratio for O^{2+} in this case is 1.8 (Table 12).

30 Doradus: We have detected lines from the 3p–3d multiplets V10, V19, V20, as well as from the 3s–3p multiplets V1, V2, V5, and several transitions from the 3d–4f group. Abundances derived from V2 and V19 agree very well with each other, but are about a factor of 2.8 higher than those derived from multiplet V1 and 88 per cent higher than those from multiplet V10. The relative intensities amongst the multiplet V19 components are in good agreement with theory (Table 7), apart from λ4156.63 (J = 5/2–3/2), which is a factor of 2 stronger than expected relative to λ4132.80 (J = 1/2–3/2), probably as a result of blending.[6] The V1 lines were discussed in the previous subsection. This abundance discrepancy is quite striking, because from observations of 10 PNe (Tsamis et al. 2002b) we have found that, on average, multiplet V2 yields O^{2+} abundances that are 24 per cent *lower* than those from V1 lines. Furthermore, O^{2+} abundances from multiplets V10 and V19 generally agree to within 40 per cent. Case dependence does not seem to be an issue because multiplets V1 and V10 are almost insensitive to optical depth effects, while it is estimated that multiplets V2 and V19, which are assumed here to be under Case B, would yield even higher abundances under Case A.

A single line from V20 is detected, λ4110.78 (J = 3/2–1/2), which yields a similar abundance to those from the V2 and V19 lines; the remaining V20 lines coincide with He I λ4120.84 and cannot be reliably used to derive an independent abundance estimate. Of the two detected multiplet V5 lines, λ4416.97 (J = 1/2–3/2) is most probably blended with [Fe II] λ4416.27 and is excluded from the analysis, while λ4414.90 (J = 3/2–5/2) yields an abundance ratio rather consistent with that from the multiplet V10 lines.

Multiplet V2 is fed from high-lying terms via $^4P^o$–^4D λ4119 (V20) and less via V19 transitions. Multiplet V19 arises from the 3d ^4P term which can be reached via resonance transitions from the O^+ $2p^3\ ^4S^o$ ground state – e.g. the $2p^3\ ^4S^o$–3d ^4P λ430 line – themselves excited by resonance fluorescence, either by starlight or by another nebular emission line. Along with resonance scattering, the excited O II 3d ^4P level will decay emitting cascade line photons

[6] This is a ratio of lines originating from the same upper level and thus invariably fixed by the ratio of their transition probabilities; the fact that it is observed to differ between several nebulae (e.g. NGC 3242, 3918, 5882, 6153 and 30 Doradus) by a factor of more than 4 suggests that blending with an unknown line affects the λ4156 line.

Table 10. Recombination line O^{2+}/H^+ abundances.[a]

λ_0 (Å)	Mult.	I_{obs}	$\frac{O^{2+}}{H^+}$ (10^{-4})
	M 17		
4638.86	V1	.1056	10.26
4641.81	V1	.1524	5.87
4649.13	V1	.1375	2.78
4650.84	V1	.0871	8.46
4661.63	V1	.1043	7.93
4676.24	V1	.0630	5.70
V1 $3s^4P - 3p^4D^o$		**0.650**	**5.41**
4317.14	V2	.1115:	14.82:
4319.63	V2	.0330	4.07
4345.56	V2	.0670	8.55
4349.43	V2	.1070	5.67
V2 $3s^4P - 3p^4P^o$		**0.207**	**5.95**
Adopted			**5.68**
	NGC 3576		
4638.86	V1	.0509	4.94
4641.81	V1	.0880	3.39
4649.13	V1	.0929	1.88
4650.84	V1	.0553	5.37
4661.63	V1	.0916	6.96
4676.24	V1	.0560	5.07
V1 $3s^4P - 3p^4D^o$		**0.435**	**3.62**
4069.62	V10	.1409:	5.45:
4072.16	V10	.1207	5.01
4075.86	V10	.1010	2.90
4085.11	V10	.1700	3.78
V10 $3p^4D^o - 3d^4F$		**0.239**	**3.77**
4087.15	V48c	.0415	13.49
4089.29	V48a	.0320	2.82
4275.55	V67a	.1339	9.85
3d-4f		**0.207**	**7.40:**
Adopted			**3.70**
	30 Doradus		
4638.86	V1	.0640	6.11
4641.81	V1	.0854	3.23
4649.13	V1	.0642	1.28
4650.84	V1	.0641	6.12
4661.63	V1	.0565	4.23
4673.73	V1	.0120	5.80
4676.24	V1	.0224	1.99
V1 $3s^4P - 3p^4D^o$		**0.369**	**2.97**
4317.14	V2	.0705	6.96
4319.63	V2	.0876	10.91
V2 $3s^4P - 3p^4P^o$		**0.158:**	**8.42:**
4414.90	V5	.0331:	6.27:
4416.97	V5	.0436:	14.8:
V5 $3s^2P - 3p^2D^o$		**0.033:**	**6.27:**
4069.89	V10	.1328	5.14
4072.16	V10	.0683	2.84
4078.84	V10	.0324	8.86
4085.11	V10	.0258	5.74
V10 $3p^4D^o - 3d^4F$		**0.259**	**4.47**
4132.80	V19	.0508	9.29
4153.30	V19	.0609	7.80
4156.53	V19	.0232:	18.6:
V19 $3p^4P^o - 3d^4P$		**0.112**	**8.41:**
4110.78	**V20**	.0322:	**13.4:**
4906.83	**V28**	.0369:	**14.8:**
4083.90	V48b	.0108	3.41
4087.15	V48c	.0185	6.17
4089.29	V48a	.0210	1.90
4275.55	V67a	.0785:	5.33:
4288.82	V53c	.1091:	11.85:
4303.83	V53a	.0519:	9.97:
4313.44	V78a	.0383:	28.5:
4315.69	V63c	.0533:	43.2:
4609.44	V92a	.0209	3.35
3d-4f		**0.071**	**3.03**
Adopted			**3.49**
	LMC N11B		
4638.86	V1	.1170	11.24
4641.81	V1	.0530	2.02
4649.13	V1	.0760	1.52
4650.84	V1	.0631	6.06
4661.63	V1	.0640	4.81
4673.73	V1	.0308	14.93
4676.24	V1	.0271	2.43
4696.35	V1	.0346	24.07
V1 $3s^4P - 3p^4D^o$		**0.466**	**3.14**
4349.43	V2	.0871	4.60
V2 $3s^4P - 3p^4P^o$		**0.087**	**4.60**
4072.16	V10	.1027	4.27
V10 $3p^4D^o - 3d^4F$		**0.103**	**4.27**
4153.30	V19	.0982	12.54
V19 $3p^4P^o - 3d^4P$		**0.098**	**12.54**
4089.29	V48a	.1305	11.41
3d-4f		**0.131**	**11.41**
Adopted			**7.19**
	SMC N66		
4638.49	V1	.0311	2.91
4649.13	V1	.0545	1.06
4650.84	V1	.0513	4.78
4661.63	V1	.0800	5.84
V1 $3s^4P - 3p^4D^o$		**0.217**	**2.15**
Adopted			**2.15**

[a]Values followed by ':' have not been used when adopting mean abundance ratios.

via the multiplets $^4S^o$–^4P λ4924 (V28), $^4P^o$–^4P λ4153 (V19) and $^4D^o$–^4P λ3907 (V11), with multiplet strength ratios of about 26.9: 18.5 : 1.0. The strongest line of V28, λ4924.53 (J = 3/2–5/2), coincides in wavelength with [Fe III] λ4924.50 and is blended with the much stronger He I λ4921.93 line at the resolution of our observations. The second strongest component of V28, λ4906.83 (J = 3/2–3/2), is detected in our spectra, yielding an even *higher* abundance ratio than the V19 lines, by 70 per cent. There is therefore marginal evidence – based on results from V28 and V19 – that the population of the 3d ^4P term is enhanced by resonance fluorescence from the ground state. This might explain the overabundances derived from these lines compared to multiplet V1 results; V1 itself is on a cascade route not affected by line fluorescent excitation. However, the single λ4110.78 (V20) line, which also produces an overabundance, yields results consistent with V19, while its upper 3d ^4D term cannot be reached via permitted transitions from the ground state. It is thus possible that stellar *continuum* fluorescence, rather than nebular *line* fluorescence is instead responsible for this pattern of intensity enhancements. From a model analysis of the permitted emission line spectrum of Orion, Grandi (1976) surmised that starlight excitation via the λ430 resonance line contributes only 20 per cent as much as recombination to the λ4153 (V19) line, while he

did not discuss the potentially worse affected λλ4906, 4924 (V28) lines; perhaps in 30 Doradus that contribution is larger. Due to their possible contamination by line or continuum fluorescence, V19 and V28 multiplet lines will be excluded from our abundance analysis.

Regarding the detected 3d–4f transitions of O II, several of these are evidently blended with [Fe II] and/or Fe II lines and have been omitted from further consideration. The 3d–4f O II ORLs are insensitive to optical depth effects and, for a significant number of PNe, their strengths have consistently proven to be in excellent agreement with theoretical predictions under an intermediate coupling scheme (cf. Liu et al. 1995a, 2000, 2001b; Tsamis et al. 2003b). From this growing body of work, it has emerged that for 11 thoroughly-analysed PNe the O^{2+}/H^+ abundance ratios derived from the best detected 3s–3p transitions (those of multiplet V1) are *lower* than those from 3d–4f lines by up to 50 per cent. This discrepancy is removed, however, if we assume that these heavy-element ORLs arise from ionized regions of very low electron temperature, of the order of $\sim 10^3$ K, much lower than those indicated by the H I recombination continuum Balmer discontinuity, just as we would expect for a dual abundance nebular model (Liu 2002b; Péquignot et al. 2002b; Tsamis 2002). Transitions of the 3d–4f group are close to hydrogenic in nature and the one amongst them with the highest total angular momentum quantum number (λ4089, upper state $J = 11/2$) is not affected by a change of coupling scheme (Storey 1994; Liu et al. 1995a). Furthermore, their upper terms cannot be reached by permitted resonance lines and are thus unaffected by fluorescence effects. Overall, the 3d–4f lines are the best ORL indicators of O^{2+}/H^+ abundances. In 30 Doradus, the strongest expected 3d–4f line at 4089.13 Å is abnormally weak compared to other 3d–4f lines (Table 7). As a consequence, the abundance ratio derived from this line alone is lower than that from the V1 lines, by 36 per cent. This is in stark contrast with the standard observed behaviour of these two sets of lines as outlined above.

An explanation for this result may involve the effect of dust-scattered stellar light on the nebular line intensities. Based on observations of the scattered light continuum described previously, we have estimated upward corrections to the observed emission line intensities for 30 Doradus (Table 9); these amount to 58 per cent (λ4072), a factor of 2.5 (λ4089), 6 per cent (λλ4638, 4640), 34 per cent (λλ4649, 4650) and 17 per cent (λ4661), respectively. The resulting corrected O^{2+}/H^+ values from the various multiplets (Table 11) then display the more regular pattern already established from the PN analysis; multiplet V1 results are now 25 per cent lower than those from the co-added 3d–4f transitions and 20 per cent lower than those from the λ4072 V10 line. Corrected line intensities and resulting O^{2+}/H^+ abundance ratios are presented in Table 11. Before any corrections, the O^{2+}/H^+ ORL abundance is 3.49×10^{-4}, while after incorporating the corrections it becomes 4.67×10^{-4}.

For 30 Doradus, the derived ORL/CEL abundance ratio for O^{2+} is 2.0 before correction for underlying stellar absorption lines; after the corrections the ratio is 2.7 (Table 12).

LMC N11B: In this nebula, too, the emission line spectrum is contaminated by the scattered continuum of illuminating stars. Regarding the nebular O II ORLs, lines of multiplet V1 are affected the most. According to our calculations presented in Tables 8 and 9, the following upward corrections to the observed nebular intensities have been estimated: 65 per cent (λ4089); 58 per cent (λλ4638, 4640); a factor of 2.1 (λλ4649, 4650); and 64 per cent (λ4661). The corrected line intensities and resulting O^{2+}/H^+ abundance ratios for this nebula are listed in Table 11. The O^{2+}/H^+ ORL abundance before any correction is 7.19×10^{-4}, while that after is 12.0×10^{-4}.

Table 11. Corrected O II intensities and resulting ORL O^{2+}/H^+ abundances.

λ_0 (Å)	Mult.	I_{cor}	$\frac{O^{2+}}{H^+}$ (10^{-4})	I_{cor}	$\frac{O^{2+}}{H^+}$ (10^{-4})
		30 Doradus		LMC N11B	
4072.16	V10	.1077	4.47	*	*
4638-40	V1	.1601	4.34	.2389	6.51
4649-50	V1	.1723	2.84	.2964	4.91
4661	V1	.0661	4.94	.1050	7.89
V1 $3s^4P - 3p^4D^o$		**0.399**	**3.59**	**0.640**	**5.26**
4083.90	V48b	.0108	3.41	*	*
4087.15	V48c	.0185	6.17	*	*
4089.29	V48a	.0531	4.79	.2154	18.8
4275.55	V53c	.0785	5.34	*	*
4609.44	V92c	.0209	3.35	*	*
3d–4f		**0.182**	**4.76**	**0.215**	**18.8**
Adopted			**4.67**		**12.0**

Therefore, for this nebula the ORL/CEL abundance ratio for O^{2+} is 4.9 before the corrections for absorption, while it rises to 8.2 afterwards (Table 12).

SMC N66: Only the V1 multiplet lines of O II are reliably detected; no corrections for underlying absorption have been estimated. Co-adding the intensities of the λ4638, λ4649, λ4650 and λ4661 transitions, we find an O^{2+}/H^+ ORL abundance ratio of 2.15×10^{-4}. The derived O^{2+} ORL/CEL ratio is 2.3 (Table 12).

5.2.3 *Uncertainties*

Clearly, even though the dust-scattered component to the observed continuum is found to be very high (~80 per cent typically) and the various absorption/emission equivalent widths were carefully measured, not *all* stars that contribute to the continuum were located. For instance, 30 Doradus contains the luminous core R136 whose effect was neglected. The missing stars most likely belong to hotter O3 If*/WN and WR types (Crowther & Dessart 1998) that have weaker O II absorption lines. Thus, for both 30 Doradus and LMC N11B, the underlying stellar absorption-line equivalent widths may be weaker than assumed here. It is therefore likely that our corrections to the observed ORL intensities and the final ORL abundances, in Table 11, are *upper* limits only in the cases of 30 Doradus and LMC N11B.

6 SPATIAL VARIATION OF NEBULAR PROPERTIES IN 30 DORADUS

The high signal-to-noise (S/N) ratio of our observations of O II ORLs from 30 Doradus (see Fig. 1) prompted us to investigate the abundance discrepancy problem in that nebula by studying the variations of electron temperature, electron density and of the ionic recombination-line C^{2+}/H^+ and O^{2+}/H^+ abundances and forbidden-line O^{2+}/H^+ abundances along the spectrograph slit. The results are presented in this section.

The 30 Doradus slit passed across the stars R139 and R140 and the nebular analysis presented thus far is based on a spectrum integrated over a spatial extent of 2 arcmin approximately. This excludes a region of 40 arcsec containing R139 and R140, in order to minimize the contribution of dust-scattered starlight to the observed spectrum. In Fig. 5 the Hβ surface brightness distribution of the nebula is plotted against the spatial dimension. Steep variations of the nebular

Table 12. ORL/CEL discrepancy factors, $\Re$, and comparison of elemental abundance ratios derived purely from ORLs and CELs.[a]

		Sun[b]	M 42[c]	M 17	NGC 3576	30 Doradus	LMC N11B	SMC N66
$10^4 \times$ O/H	(CELs)	4.90	3.32	3.59	3.31	2.17	2.59	1.28
$\Re(O^{2+})$	(ORL/CEL)	*	1.3	2.1	1.8	2.0–2.7	4.9–8.2	2.3
$\Re(C^{2+})$	(ORL/CEL)	*	2.4	*	*	2.6[d]	*	*
C^{2+}/O^{2+}	(ORLs)[e]	0.50	0.77	0.77	0.78	0.25	0.25	$\lesssim 0.20$
N^{2+}/O^{2+}	(ORLs)[e]	0.19	0.15	0.62	0.71	$\lesssim 0.16$	*	*
N^{2+}/O^{2+}	(IR CELs)[f]	0.19	0.19	0.19	0.16	0.060	0.075	*
N^{+}/O^{+}	(CELs)	0.19	0.15	0.088	0.11	0.036	0.033	0.016
Ne/O	(CELs)	0.25	0.18	0.28	0.16	0.21	0.16	0.18
S/O	(CELs)	0.033	0.028	0.027	*	0.027	0.019:	0.018
Ar/O	(CELs)	.0074	.011	.0057	.0078	.0065	.0078	.0053
$10^4 \times O^{2+}/H^{+}$	(Opt CELs)	*	2.26	2.66	2.21	1.76	1.47	0.94
$10^4 \times O^{2+}/H^{+}$	(IR CELs)[g]	*	1.66	1.80	2.68	2.21	*	*

[a]All nebular data are from this paper, apart from those in rows 6 and 12, and the data in rows 7–10 for M42.
[b]Solar elemental ratios, adopting log (X/H) + 12.0 = 8.69 and 8.39 for X = O and C from Allende Prieto et al. (2001, 2002), together with N, Ne, S and Ar abundances from Grevesse, Noels & Sauval (1996).
[c]Entries 1–5 and entry 11 from our unpublished data; entries 7–10 from Esteban et al. (1998).
[d]Adopting a CEL C^{2+}/H^{+} abundance of 3.44×10^{-5} from Dufour et al. (1982).
[e]No corrections for scattered light absorption features have been implemented in obtaining the listed nebular ORL C^{2+}/O^{2+} and N^{2+}/O^{2+} ratios.
[f]From Simpson et al. (1995) for M 17, NGC 3576 and 30 Dor; from Rubin et al. (1988) for M 42; value for LMC N11B derived from the [O III] 52- and 88-μm and [N III] 57-μm fluxes in ISO LWS spectrum TDT60901217. Note that the positions at which these IR data were obtained were not the same as for our optical long-slit spectra.
[g]From Simpson et al. (1995) for M 17, NGC 3576 and 30 Dor; from Rubin et al. (1991) for M 42.

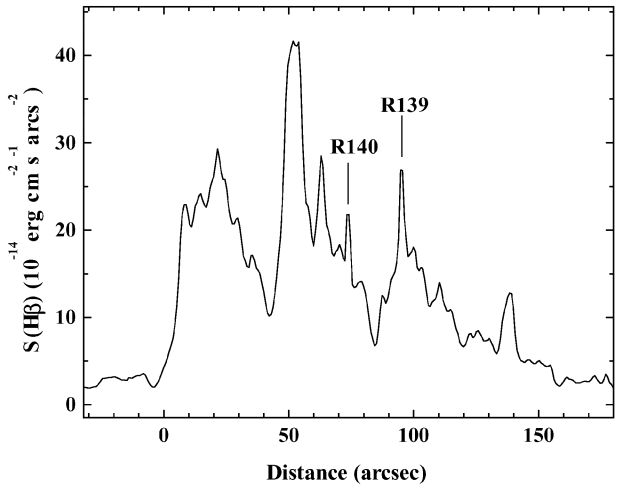

Figure 5. The Hβ surface brightness distribution of 30 Doradus along the slit; interstellar extinction has not been corrected for. The positions of the R139 and R140 systems are marked.

surface brightness are seen. The positions corresponding to R140 and R139 are at +73 and +95 arcsec, respectively.

For the blue spectra, each pixel along the slit corresponded to 0.74 arcsec on the sky, while the seeing was about 1 arcsec FWHM. For the spatial analysis we used spectra secured with the two overlapping grating set-ups, centred at 4290 Å, covering the C II λ4267 recombination line, Hγ and the [O III] λ4363 CEL, and at 4745 Å, covering the O II V 1 recombination multiplet at 4650 Å, the [Ar IV] λλ4711, 4740 density-sensitive doublet, Hβ and the [O III] λ4959 forbidden line. For each grating set-up, spectra were extracted at intervals along the slit, averaged over about five pixels each time, so that a substantial S/N ratio was achieved. We wanted to examine the nebular properties as close as possible to stars such as R139 and R140, so spectra were also extracted in the region between the two, which was not included previously in the integrated spectrum. The individual extractions were brought to scale via their overlapping portions and normalized to flux units such that $F(H\beta) = 100$. We then subtracted the local continuum and measured the fluxes of C II λ4267 and O II V1 multiplet recombination lines, as well as the [Ar IV] doublet and [O III] λλ4363, 4959 CELs, dereddening them using the extinction constant derived from the integrated spectrum (Section 3.1).

The electron temperature derived from the [O III] λ4959/λ4363 ratio, as a function of position along the slit, is shown in Fig. 6. The [O III] λ4959 line was saturated on the four 20-min exposures centred at 4745 Å, so its flux was measured on the 5-min high-resolution spectrum. The [O III] temperature is found to remain practically constant over the region examined here, with a mean value of 9990 K and a standard deviation of 200 K. This is marginally lower than the temperature of 10 100 ± 250 K, derived using the line fluxes from the integrated spectrum (Table 3). No evidence for substantial temperature fluctuations is seen.

The electron density variation across the nebula has been mapped using the [Ar IV] doublet ratio and is plotted in Fig. 6 as well. The density has a mean value of 1960 cm^{-3} and a standard deviation of 1220 cm^{-3}. This is in good agreement with the [Ar IV] density of 1800 cm^{-3} derived from the integrated spectrum (Table 3). There is evidence for a density minimum of $N_e = 100$ cm^{-3} at +40 arcsec in Fig. 6, corresponding to a local minimum in the Hβ surface brightness at about +40 arcsec in Fig. 5. Owing to the high critical densities of the λλ4711, 4740 transitions (14 000 and 130 000 cm^{-3} respectively), the [Ar IV] lines are good tracers of high-density ionized gas, while still sensitive down to $N_e \sim 10^3$ cm^{-3}. We see no evidence, however, of any high-density material at our spatial resolution.

In Fig. 7 the variation of the He^{+}/H^{+} abundance ratio across the 30 Doradus nebula is presented, derived from the He I λ4471

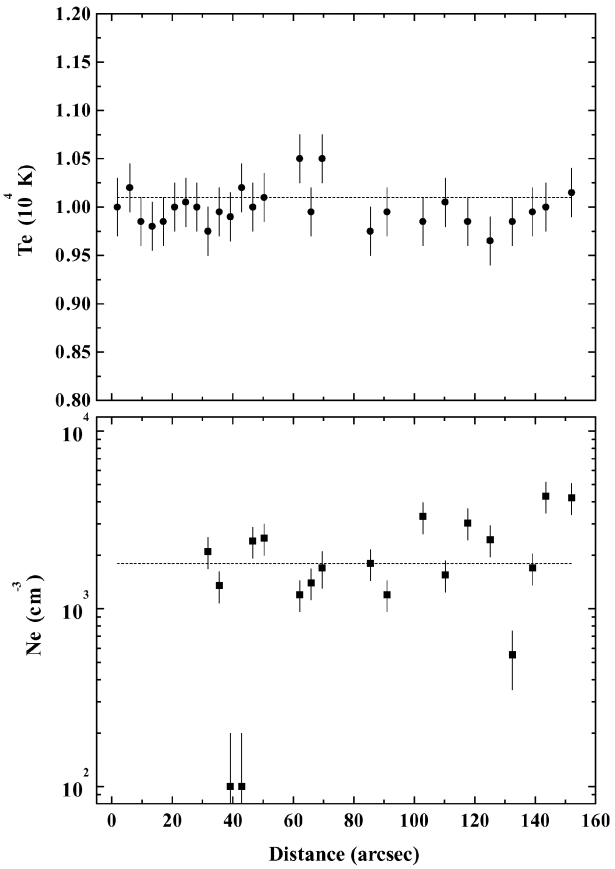

Figure 6. Top panel: Variations of the electron temperature in 30 Doradus derived from [O III] λ4959/λ4363. The dashed line denotes the temperature derived from line fluxes obtained from integrating the spectrum along the slit. Bottom panel: The electron density derived from [Ar IV] λ4740/λ4711, with the dashed line having the same meaning as previously.

recombination line. The adopted electron temperature was 9990 K. The He^+/H^+ ratio remains constant over the range plotted here. The helium abundance remains very close to the mean value even in the nebular region between R139 and R140.

Fig. 8 shows the spatial variations of the C^{2+}/H^+ and O^{2+}/H^+ ORL abundances and of the O^{2+}/H^+ forbidden-line abundance, derived respectively from the C II λ4267 line, the O II V1 multiplet at 4650 Å and the [O III] λ4959 forbidden line. In should be noted that, in order to circumvent non-LTE effects that affect abundances derived from individual O II V1 components (Section 5.2.1), the total observed intensity of the λ4650 multiplet was used to obtain the ORL O^{2+}/H^+ ratio. An electron temperature of 9990 K was adopted for the calculation of the ORL abundances, while the point-by-point [O III] λ4959/λ4363 temperature measurements (Fig. 6) were used for the derivation of the forbidden-line O^{2+}/H^+ values.

From Fig. 8 (top panel) no significant variation in the *forbidden*-line O^{2+}/H^+ abundance across the nebula can be discerned. Over the whole range plotted, O^{2+}/H^+ has an average value of 1.83×10^{-4} and a standard deviation of 1.10×10^{-5}. The forbidden-line abundance remains consistently lower than the ORL O^{2+}/H^+ abundance across the plotted range, by a factor of 2. The C^{2+}/H^+ abundance derived from the collisionally-excited C III] λ1908 intercombination doublet (Dufour, Shields & Talbot 1982) is also consistently lower than the mapped ORL abundances of doubly ionized

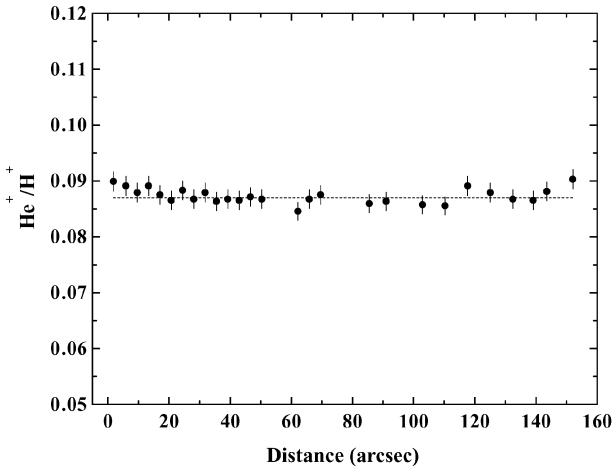

Figure 7. Variation of the He^+/H^+ abundance ratio along the slit for 30 Doradus, derived from the He I λ4471 line. The dashed line marks the helium abundance derived from integrating the λ4471 flux along the slit.

carbon. Could temperature fluctuations account for these discrepancies? At the spatial resolution of our mapping, there is no evidence of [O III] temperature fluctuations of a sufficient magnitude to cause this. An electron temperature of 8200 K would be needed in order to force the forbidden-line O^{2+}/H^+ abundances to become equal to the recombination-line abundances. This would necessitate the existence of fluctuations from the mean temperature (9990 K) of about 18 per cent or – in the terminology of Peimbert (1967) – a temperature fluctuation parameter $t^2 \sim 0.03$, which is however not deduced from our spatial analysis. We note, however, that while the above observations place constraints upon temperature fluctuations in the plane of the sky, along our slit, fluctuations along the line of sight though the nebula are not constrained by this method. Rubin et al. (2002) discuss this point in more detail, in the context of *HST* observations of the planetary nebula NGC 7009.

Fig. 8 also presents, for the first time to our knowledge for an extragalactic H II region, the spatial variation of the C^{2+}/O^{2+} ratio derived purely from ORLs. The C^{2+}/O^{2+} ratio across the nebula has a mean value of 0.33 and a 1σ error of 0.02. This is in excellent agreement with the value of 0.30 derived from the integrated spectrum. This latter value was calculated adopting as the O^{2+}/H^+ abundance the value derived from the V1 multiplet (Table 10), while the mean C^{2+}/H^+ abundance is taken from Table 5. The O^{2+} V1 abundances that were used for Fig. 8 are those *before* any correction is made for underlying absorption at 4650 Å in the scattered-light continuum. Such a correction is estimated to raise the O^{2+} recombination-line abundance by a factor of 1.34 (Section 5.2.2). An interesting feature of our spatial analysis of heavy-element ORLs is that there is tentative evidence for a local minimum in the C^{2+}/O^{2+} ratio, derived purely from ORLs, in the nebular region between the massive stars R139 and R140. The relevance of this result is discussed in the following section.

7 DISCUSSION

7.1 ORL/CEL abundance discrepancies and elemental ratios

It is clear from the above analysis and Table 12 that substantial ORL versus CEL abundance discrepancies *are present*, not only in planetary nebulae, but also in H II regions.

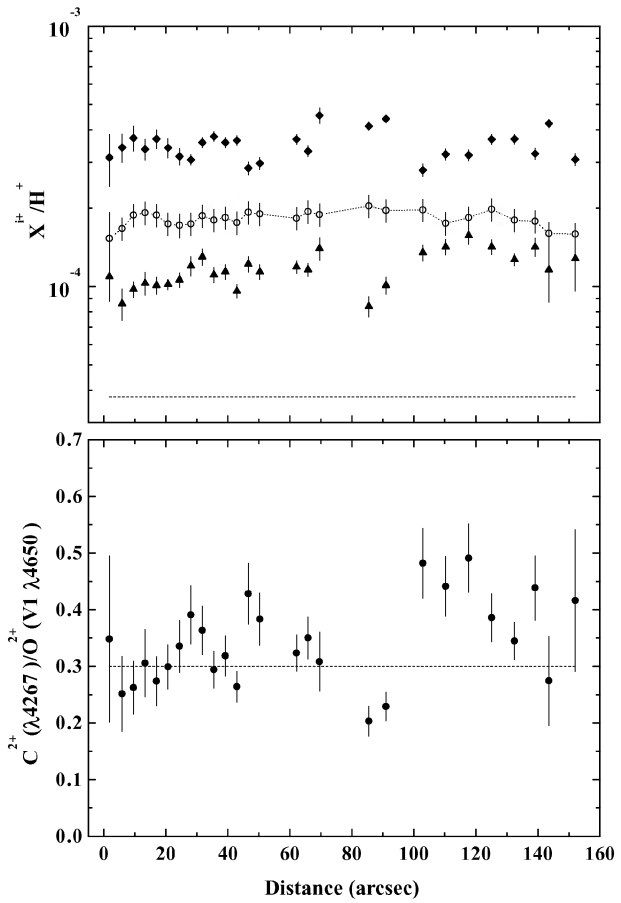

Figure 8. Top panel: Variations across 30 Doradus of the ionic *recombination*-line abundance of O^{2+}/H^+ (solid diamonds) derived from the O II V1 multiplet at 4650 Å, the ionic *forbidden*-line abundance of O^{2+}/H^+ (open circles, dotted line) derived from the [O III] λ4959 line, and the ionic recombination-line abundance of C^{2+}/H^+ (solid triangles) derived from the C II λ4267 line. The horizontal dashed line at the bottom denotes the *forbidden*-line abundance of C^{2+}/H^+ derived from the C III] λ1909 doublet using the line intensity quoted by Dufour et al. (1982). Bottom panel: The C^{2+}/O^{2+} ratio derived solely from *recombination*-lines. The dashed line denotes the ratio obtained from the integrated spectrum.

Discrepancies were reported for M 42 and M 17 by Peimbert et al. (1993), for both of which they found an ORL/CEL factor of ∼1.7 for the O^{2+} ion. Esteban et al. (1998) found ORL/CEL discrepancy factors of 1.4–1.6 and 2.2, respectively, for O^{2+} and C^{2+} in the Orion nebula; adopting $C^{2+}(\lambda1908)/H^+$ CEL abundances from Walter, Dufour & Hester (1992). Our unpublished long-slit spectra, obtained at the AAT 3.9-m and ESO 1.52-m telescopes, show a factor of only 1.3 discrepancy for O^{2+} in that nebula, but imply an ORL/CEL C^{2+} discrepancy of 2.4, when compared with the *IUE* results of Walter et al. for C III] λ1908. For the H II region M 8, Esteban et al. (1999) reported a factor of 2 discrepancy between the recombination-line O^{2+} abundance and its forbidden-line value. A CEL abundance study of the Gum 38a complex, which contains NGC 3576, has been made by Girardi et al. (1997), but no detection of C II λ4267 or any other heavy-element optical recombination line was reported. Owing to its high reddening, NGC 3576 was never observed by the *IUE* either, so no comparison can be made with the ORL C^{2+}/H^+ abundance ratio reported here.

Table 12 shows that the ORL/CEL O^{2+} discrepancy factors, $\Re$, for our H II regions are 2.1, 1.8, 2.0–2.7, 4.9–8.2 and 2.3 for M 17, NGC 3576, 30 Doradus, LMC N11B and SMC N66, respectively. Even if we adopt the lower ORL abundances for 30 Doradus and N11B (i.e. neglecting corrections for any underlying absorption in the dust-scattered continuum), the mean discrepancy factor is 2.6. LMC N11B displays the largest discrepancy documented so far for an H II region (=4.9), in the neighbourhood of the mean value (=5.1) that we have found for a sample of 18 PNe (Tsamis et al. 2003b). How can we explain such an extreme discrepancy for an H II region?

Before commenting on this issue, we consider the derived elemental abundance ratios presented in Table 12 for this sample of H II regions, where they are compared with solar values. The C^{2+}/O^{2+} and N^{2+}/O^{2+} ratios are purely from ORL lines and should be almost completely unaffected by temperature variations. They should give a good measure of the C/O and N/O ratios – especially the latter as, for these relatively high-excitation H II regions, the N^{2+} and O^{2+} zones occupy almost the entire H^+ zone (Shaver et al. 1983; Simpson et al. 1995). From Table 12, we see that the agreement between the C^{2+}/O^{2+} ratios for the three galactic nebulae is excellent, with the mean value of 0.77 being 50 per cent higher than the solar value of Allende Prieto, Lambert & Asplund (2001, 2002).

The ORL N^{2+}/O^{2+} and CEL N^{2+}/O^{2+} and N^+/O^+ ratios listed for M 42 in Table 12 are in good agreement. Our N^{2+}/O^{2+} ORL results for M 17 and NGC 3576 are much *higher* than the respective CEL N^{2+}/O^{2+} ratios, by factors of 3–4.5, while they are also larger than the N^+/O^+ CEL ratios. There is the strong possibility, however, that the N II ORLs used for these two nebulae yield unreliable abundances because they are affected by fluorescence effects. Grandi (1976) showed that, for Orion, the N II multiplets V3, V5 and V30 are excited by fluorescence via the He I λ508.6 resonance line. In the current study, N^{2+}/H^+ abundances for M 17 and NGC 3576 have been derived from N II multiplets V3 and V5 (Table 6). On the other hand, Liu et al. (2001b) showed that the observed N II ORL intensity ratios for the planetary nebulae M 1-42 and M 2-36 are inconsistent with fluorescent *line*-excitation of the N II V3 and V5 lines. They proposed that continuum fluorescence by starlight is a more plausible cause. In any case, it seems probable that fluorescence of some sort contributes to the excitation of the N II V3 and V5 triplet lines observed from M 17 and NGC 3576. Unfortunately, the N II 3d–4f high-lying transitions, which are generally not biased by this effect, have not been detected from either M 17 or NGC 3576; their measurement would offer a means of checking the fluorescence hypothesis. However, the ORL N^{2+}/O^{2+} ratio for M 42 listed in Table 12 was based on our observations of N II 3d–4f and singlet lines, and so should be unaffected by fluorescence effects, consistent with the agreement found between the ORL N^{2+}/O^{2+} and CEL N^{2+}/O^{2+} and N^+/O^+ ratios for this nebula.

For the two LMC nebulae, the C^{2+}/O^{2+} ORL ratios are in excellent agreement, their value of 0.25 being only 11 per cent smaller than the mean CEL C/O ratio of 0.28 found for LMC H II regions by Kurt & Dufour (1998). In addition, their N^+/O^+ ratios are in excellent agreement with the mean CEL N/O ratio of 0.035 for the LMC found by the same authors, though smaller than the N^{2+}/O^{2+} ratios found for the same two nebulae from far-infrared (FIR) CELs. Finally, for SMC N66, our C^{2+}/O^{2+} ORL upper limit is consistent with the SMC mean CEL C/O value of 0.15 (Kurt & Dufour 1998), although our CEL N^+/O^+ ratio of 0.016 is only 46 per cent of the mean CEL N/O ratio of 0.035, of Kurt & Dufour, for the SMC.

From the above comparisons, an important conclusion can be drawn. It seems that the C/O abundance ratio derived from ORLs is

equal within the uncertainties to the same ratio derived from CELs, both for the galactic nebulae and, as quoted by Kurt & Dufour, for the Magellanic Cloud nebulae as well (a similar conclusion appears to apply to N/O ratios too, provided care is taken in the choice of the N II ORLs used to derive N^{2+} abundances). Similar results for C/O, N/O and Ne/O have been reported for planetary nebulae (Liu et al. 1995a, 2000, 2001b; Mathis, Torres-Peimbert & Peimbert 1998; Luo et al. 2001). Apart from the obvious observation that this strengthens the reliability of C/O or N/O ratios derived from either pure CEL or pure ORL abundance analyses, it also raises important questions regarding the chemical history of the ORL-emitting medium with respect to that of the 'normal' CEL-emitting nebular component, given that they appear to have similar C/O, N/O and Ne/O ratios.

7.2 Potential causes of the ORL/CEL abundance discrepancies

7.2.1 The case against temperature fluctuations

The existence of temperature fluctuations within the nebular volumes has been long thought to offer an obvious solution to the conundrum of discrepant ORL versus CEL abundances, both for PNe and H II regions. Temperature fluctuations within a nebula can lead to enhanced emission of the temperature-sensitive, high-excitation energy [O III] λ4363 transition from the hotter nebular regions. As a result, the electron temperature deduced from the net [O III] (λ4959 + λ5007)/λ4363 intensity ratio would be biased towards the hotter regions and would lead to too low an O^{2+} abundance being derived from the net nebular spectrum. The Peimbert (1967) temperature fluctuation parameter, t^2, derived from a comparison between the hydrogen BJ and [O III] forbidden-line temperatures, is 0.011 and 0.017 for M 17 and NGC 3576, respectively (Table 3). On the other hand, the ORL/CEL O^{2+} discrepancy factors for these two nebulae of 2.1 and 1.7, respectively, would require values of $t^2 \sim 0.038$, i.e. considerably larger.[7] For the three Magellanic Cloud nebulae, the t^2 factors implied by the abundance discrepancies are even greater, reaching the uncomfortably high value of ~0.1 in the case of LMC N11B, very similar to the value needed to reconcile ORL and CEL O^{2+} abundances for the rather extreme planetary nebula NGC 7009 (Liu et al. 1995a). This is a factor of 10 larger than typical values predicted by photoionization models of chemically and density homogeneous nebulae, which yield $t^2 \sim 0.01$ (Garnett 1992; Gruenwald & Viegas 1995; Kingdon & Ferland 1995b). As in the case of planetary nebulae, it seems unlikely that temperature fluctuations are to blame for the discrepancies observed here, especially for extreme objects such as LMC N11B.

If temperature fluctuations were indeed responsible for the low heavy-element ion abundances deduced from optical CELs compared to those derived from ORLs (see rows 2 and 3 of Table 12), we would then expect IR CELs to yield abundances similar to the high values obtained from ORLs, due to the low excitation energies of IR fine-structure transitions and their consequent lack of sensitivity to temperature fluctuations at typical nebular temperatures. The last two rows of Table 12 compare O^{2+}/H^+ CEL abundances derived from our optical spectra with those derived by Rubin et al. (1988) and Simpson et al. (1995) from IR fine-structure line observations of four of the nebulae. For M 42 and M 17, the IR CEL lines yield O^{2+}/H^+ abundances which are 27 and 32 per cent smaller than those obtained from our optical CEL observations, while for NGC 3576 and 30 Doradus the IR CEL lines yield O^{2+}/H^+ abundances which are 21 and 26 per cent larger than those from the optical CEL data. These differences of only 20–30 per cent are close to the 20 per cent uncertainties estimated by Simpson et al. for the radio free–free fluxes (that measure H^+) falling in the Kuiper Airborne Observatory (KAO) beam used for the FIR line observations. It should be noted that the positions in the nebulae that were observed at FIR wavelengths with the KAO usually did not coincide with the positions covered by our optical long-slit observations. However, spatial abundance variations within these H II regions have never been detected, as exemplified by our own spatially-resolved abundance analysis of 30 Dor (Section 6).

We therefore conclude that the agreement found between the O^{2+}/H^+ abundances derived from optical and IR CELs rules out temperature fluctuations as the cause of the factor of 2 discrepancy found between ORL and CEL O^{2+}/H^+ abundances for M 17, NGC 3576 and 30 Doradus. On the other hand, the large t^2 derived for LMC N11B from the ORL/CEL O^{2+} ratio would imply temperature fluctuations that cannot be explained by chemically and density homogeneous nebular models.

7.2.2 The case against high-density clumps and in favour of metal-rich inclusions

High-density ionized clumps with $N_e \geqslant 10^5$ cm^{-3} embedded in a medium of lower density could lead to low CEL C, N and O abundances, via an effect of pseudo-temperature fluctuations, whereby the observationally derived [O III] temperature is significantly overestimated due to collisional quenching of the nebular λλ4959, 5007 lines (Viegas & Clegg 1994). Such high-density clumps would also quench emission in the low critical density FIR lines of [O III] and [N III], leading to lower abundances being deduced from IR CELs than from ORLs.

HST images of the Orion nebula show numerous clumpy microstructures surrounded by more or less uniform nebulosity. Walsh & Rosa (1999) reported *HST* observations of a partially ionized globule and a filament in the Orion nebula that displays high densities of up to 5×10^6 cm^{-3}. They did not however publish the density-sensitive diagnostic. They also commented that in the core of the nebula the filaments contribute half the [N II] emission, but only 10 per cent of the Balmer line flux. The existence of high-density, partially ionized condensations with $N_e \sim 10^6$ cm^{-3} has also been postulated by Bautista, Pradhan & Osterbrock (1994) in order to explain abnormalities in the emission spectrum of [Fe II] in the Orion nebula. Independent observations by Esteban et al. (1998) and Baldwin et al. (2000), however, have shown that [Fe II] lines are formed in lower-density gas along with [O I] lines. Finally, as Lucy (1995) and Verner et al. (2000) discuss, the formation of [Fe II] emission lines is affected by radiative pumping fluorescence processes in ways that render them unsuitable as straightforward density diagnostics for H II regions.

In Fig. 9 we plot the reddening-corrected intensities of high-order H I Balmer lines from our high-resolution (1 Å) spectrum of NGC 3576 and compare them with theoretical predictions for various nebular electron densities (Storey & Hummer 1995). Since such lines are sensitive indicators of ionized, high-density regions (assuming those have a normal hydrogen content), it is interesting to see that our data do not show any evidence for significant amounts of high-density material. In fact, the spectrum can be fitted with a uniform electron density of 3000 cm^{-3}, consistent with the values

[7] On the other hand, Liu et al. (1995b) found very similar values of T_e(O III) and T_e(BJ) for M 42, the nebula in Table 12 with the smallest O^{2+} ORL/CEL discrepancy factor (=1.3).

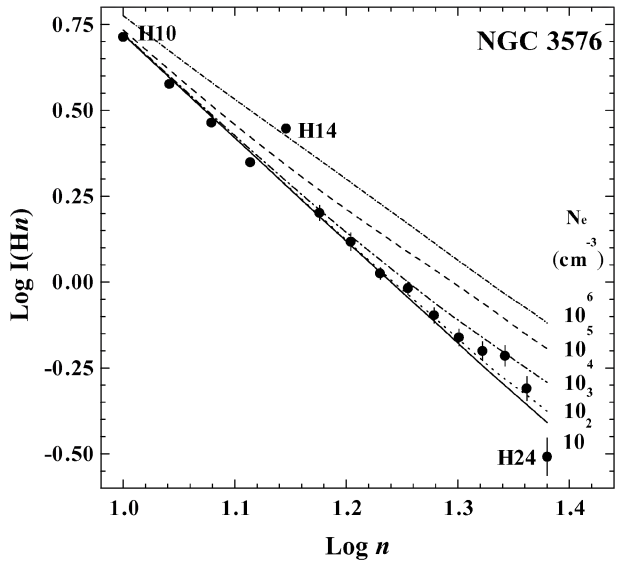

Figure 9. Observed log-intensities (in units of Hβ = 100) of high-order Balmer lines ($n \rightarrow 2$, $n = 10, \ldots, 24$) as a function of the principal quantum number n; H 14 at 3721.94 Å is blended with the [S III] λ3721.63 line. The various curves show, respectively, the predicted Balmer decrements for electron densities from $N_e = 10^2$ to 10^6 cm^{-3}. A constant temperature of 8070 K, derived from the nebular continuum Balmer discontinuity, has been assumed in all cases.

derived from the optical [Cl III] density diagnostics (Section 3.2, Table 3). We note that our adopted reddening of c(Hβ) = 1.25 for NGC 3576 was derived from the observed relative intensities of Hα, Hβ, Hγ and Hδ. The dereddened intensities of these low Balmer lines give an excellent fit to the theoretical Case B ratios (Table 2). The high Balmer lines (H10–H24) used for Fig. 9 span a wavelength range of less than 130 Å, so it would require a large change in the adopted reddening to change their decrement slope to one that was consistent with $N_e = 10^5$–10^6 cm^{-3}. However, such a change in reddening would be inconsistent with the low Balmer line relative intensities. We consider the high-n Balmer lines to provide a secure upper limit of $N_e < 10^4$ cm^{-3} for their emitting region.

The Balmer decrement electron density diagnostic discussed above pertains to regions dominated by hydrogen, but not necessarily to possible hydrogen-deficient regions in the nebulae, which could give rise to enhanced heavy-element ORL emission, causing the observed abundance discrepancies. However, such hydrogen-deficient regions cannot have electron densities significantly higher than those deduced from the hydrogen Balmer decrement, in the case of NGC 3576, or from the standard CEL density diagnostics discussed in Section 3.2, because, as discussed in Section 5.2.1, the observed relative intensities of O II V1 multiplet components indicate that O^{2+} recombination is occurring in regions with electron densities lower than 3500 cm^{-3}, the critical density of the O^{2+} $^3P_2$ level. Collisional quenching of the optical and IR CELs in high-density clumps can therefore be ruled out as the cause of the lower abundances derived from CELs compared to those derived from ORLs. The only remaining way in which CELs can be collectively suppressed in an ORL-emitting ionized region is for the temperature of the region to be low enough to suppress not just optical CEL emission but also IR fine-structure emission lines such as the 52- and 88-μm lines of [O III], implying electron temperatures lower than a few hundred Kelvin. Is there any evidence for hydrogen-deficient zones inside H II regions?

Rosa & Mathis (1987) have reported on the existence of a hydrogen-poor (He/H = 0.14) region in the outskirts of the 30 Doradus nebula, enhanced in most metals, apart from nitrogen. They hypothesize that it might contain chemically processed ejecta from a massive, late-type Wolf–Rayet star. It would be interesting to obtain high spatial resolution spectra of that region to search for regions of enhanced heavy-element ORL emission. Our long-slit spectra sample a slice through the central 1 arcmin of 30 Doradus, which is known to contain a number of WR stars (Moffat et al. 1987; Parker 1993). Could it be that knots of heavy-element enriched material have been ejected from such stars and are the cause of the high ORL abundances? It is well known from kinematical studies (e.g. Meaburn 1984) that 30 Doradus contains pressure-driven bubbles, shells and sheets of ionized gas, originating from interactions with the intense winds from WR, Of stars and supernova remnant ejecta. In fact, two such potential culprits were directly encountered by our long slit, i.e. R139 (Of + WNL-type) and R140 (WC + WN-type). The existence of a local minimum in the ORL C^{2+}/O^{2+} ratio (Fig. 8) in the nebular region between R139 and R140 might be indicative of an outflow of carbon-depleted material from these evolved stars. On the other hand, LMC N11B does not contain any known Wolf–Rayet stars (Parker et al. 1992) and its ORL/CEL abundance discrepancy factor is more than twice that of 30 Doradus. Moreover, the fact that amongst our sample of H II regions the ORL C^{2+}/O^{2+} ratios of the postulated hydrogen-deficient component are so similar to the CEL C/O ratios of the 'normal' nebular component seems hard to reconcile with standard nuclear-processing scenarios for the hydrogen-deficient component.

Concerning the apparent low-density of the ORL-emitting material, it is interesting to make a comparison with the dual-component nebular models of the PN NGC 6153 (Liu et al. 2000), proposed as a solution for the extreme ORL/CEL abundance discrepancy (a factor of 10) in that nebula. One of those models (IH2) contained very cold (500 K), low-density (<1000 cm^{-3}) H-deficient inclusions, immersed in hot gas with normal abundances. This model, however, was rejected for NGC 6153 on account of (a) the required large filling factor of the metal-rich component, which would significantly increase the total CNO content of the nebula, and (b) the very large overpressure of the normal component, which would lead to the rapid collapse of the postulated inclusions. It is possible that the O II ORLs from our sample of H II regions originate from cold, low-density, ionized and metal-rich regions located around much denser neutral cores, which may also be H-deficient; such material may have been ejected from evolved, massive Of/WR stars in the vicinity. The existence of *neutral*, dense inclusions, whose photo-evaporation leads to the emission of heavy-element ORLs from lower-density ionized haloes, could help to alleviate the problem of the survival of fully ionized inclusions subject to large overpressures.

8 CONCLUSIONS

The current data set supported by published FIR observations all but rules out the notion that Peimbert-type temperature fluctuations are the cause of the high metal abundances derived from optical recombination lines with respect to the lower abundances yielded by forbidden lines in H II regions. Neither do our results advance the case for the existence of Viegas & Clegg-type *high-density, ionized* condensations in this sample of nebulae that could compromise the observationally derived [O III] temperature, because the relative intensities of high-order H I Balmer lines *and* the relative intensities

of O II V1 multiplet components both indicate that recombination is occurring in regions having electron densities similar to those indicated by the standard CEL nebular density diagnostics. Instead, our analysis points towards an origin for much of the enhanced heavy-element optical recombination-line emission (enhanced relative to the optical and IR CEL lines from the same ions) in ionized regions that are of *low* density and which are also cold, so that they do not emit CELs. Thus, a resolution of the ORL/CEL problem appears to require the existence of a hitherto unseen component in these H II regions, consisting of cold, rarefied and metal-rich, ionized gas.

ACKNOWLEDGMENTS

YGT acknowledges the award of a Perren Studentship. We thank Daniel Péquignot for insightful comments and helpful discussions and the referee, Dr R. Rubin, for his very careful reading of the manuscript.

REFERENCES

Allende Prieto C., Lambert D. L., Asplund M., 2001, ApJ, 556, L63
Allende Prieto C., Lambert D. L., Asplund M., 2002, ApJ, 573, L137
Baldwin J. A., Verner E. M., Verner D. A., Ferland G. J., Martin P. G., Korista K. T., Rubin R. H., 2000, ApJS, 129, 229
Bautista M. A., Pradhan A. K., Osterbrock D. E., 1994, ApJ, 432, 135
Brocklehurst M., 1972, MNRAS, 157, 211
Brown R. L., Mathews W. G., 1970, ApJ, 160, 939
Burstein D., Heiles C., 1982, AJ, 87, 1165
Crowther P. A., Dessart L., 1998, MNRAS, 296, 622
Dufour R. J., Shields G. A., Talbot R. J., Jr., 1982, ApJ, 252, 461
Esteban C., Peimbert M., Torres-Peimbert S., Escalante V., 1998, MNRAS, 295, 401
Esteban C., Peimbert M., Torres-Peimbert S., García-Rojas J., Rodríguez M., 1999, ApJS, 120, 113
Garnett D. R., 1992, AJ, 103, 1330
Garnett D. R., Dinerstein H. L., 2001, ApJ, 558, 145
Girardi L., Bica E., Pastoriza M. G., Winge C., 1997, ApJ, 486, 847
Grandi S. A., 1976, ApJ, 206, 658
Grevesse N., Noels A., Sauval A. J., 1996, in Holt S. S., Sonneborn G., eds, ASP Conf. Ser. Vol. 99, Cosmic Abundances. Astron. Soc. Pac., San Francisco, p. 117
Gruenwald R., Viegas S. M., 1995, A&A, 303, 535
Hamuy M., Suntzeff N. B., Heathcote S. R., Walker A. R., Gigoux P., Phillips M. M., 1994, PASP, 106, 566
Henry R. B. C., Kwitter K. B., Bates J. A., 2000, ApJ, 531, 928
Hill J. K. et al., 1993, ApJ, 413, 604
Howarth I. D., 1983, MNRAS, 203, 201
Kingdon J., Ferland G. J., 1995a, ApJ, 442, 714
Kingdon J., Ferland G. J., 1995b, ApJ, 450, 691
Kingsburgh R. L., Barlow M. J., 1994, MNRAS, 271, 257
Kurt C. M., Dufour R. J., 1998, Rev. Mex. Astron. Astrofis., 31, 147
Liu X.-W., 2002a, Rev. Mex. Astron. Astrof., Ser. de Conf., 12, 70
Liu X.-W., 2002b, in Sutherland R., Kwok S., Dopita M. A., eds, Proc. IAU Symp. 209, Planetary Nebulae. Astron. Soc. Pac., San Francisco, in press
Liu X.-W., Storey P. J., Barlow M. J., Clegg R. E. S., 1995a, MNRAS, 272, 369
Liu X.-W., Barlow M. J., Danziger I. J., Storey P. J., 1995b, ApJ, 450, L59
Liu X.-W., Storey P. J., Barlow M. J., Danziger I. J., Cohen M., Bryce M., 2000, MNRAS, 312, 585
Liu X.-W. et al., 2001a, MNRAS, 323, 342
Liu X.-W., Luo S.-G., Barlow M. J., Danziger I. J., Storey P. J., 2001b, MNRAS, 327, 141
Lucy L. B., 1995, A&A, 294, 555
Luo S.-G., Liu X.-W., Barlow M. J., 2001, MNRAS, 326, 1049
Mathis J. S., Torres-Peimbert S., Peimbert M., 1998, ApJ, 495, 328
Meaburn J., 1984, MNRAS, 211, 521
Moffat A. F. J., 1989, ApJ, 347, 373
Moffat A. F. J., Niemela V. S., Chu Y.-H., Seggewiss W., 1987, ApJ, 312, 612
Parker J. W., 1993, AJ, 106, 560
Parker J. W., Garmany C. D., Massey P., Walborn N. R., 1992, AJ, 103, 1205
Peimbert M., 1967, ApJ, 150, 825
Peimbert M., Storey P. J., Torres-Peimbert S., 1993, ApJ, 414, 626
Péquignot D., Amara M., Liu X.-W., Barlow M. J., Storey P. J., Morisset C., Torres-Peimbert S., Peimbert M., 2002a, Rev. Mex. Astron. Astrof., Ser. de Conf., 12, 142
Péquignot D., Liu X.-W., Barlow M. J., Storey P. J., Morisset C., 2002b, in Sutherland R., Kwok S., Dopita M. A., eds, Proc. IAU Symp. 209, Planetary Nebulae. Astron. Soc. Pac., San Francisco, in press
Rosa M., Mathis J. S., 1987, ApJ, 317, 163
Rubin R. H., 1986, ApJ, 309, 334
Rubin R. H., 1989, ApJS, 69, 897
Rubin R. H., Simpson J. P., Erickson E. F., Haas M. R., 1988, ApJ, 327, 377
Rubin R. H., Simpson J. P., Haas M. R., Erickson E. F., 1991, ApJ, 374, 564
Rubin R. H. et al., 2002, MNRAS, 334, 777
Shaver P. A., McGee R. X., Newton L. M., Danks A. C., Pottasch S. R., 1983, MNRAS, 204, 53
Shields G. A., 2002, Rev. Mex. Astron. Astrof., Ser. de Conf., 12, 142
Simpson J. P., Colgan S. W. J., Rubin R. H., Erickson E. F., Haas M. R., 1995, ApJ, 444, 721
Smits D. P., 1996, MNRAS, 278, 683
Stasińska G., 1980, A&A, 84, 320
Storey P. J., 1994, MNRAS, 282, 999
Storey P. J., Hummer D. G., 1995, MNRAS, 272, 41
Tsamis Y. G., 2002, PhD thesis, University of London
Tsamis Y. G., Liu X.-W., Barlow M. J., Danziger I. J., Storey P. J., 2003a, MNRAS, submitted
Tsamis Y. G., Liu X.-W., Barlow M. J., Storey P. J., Danziger I. J., 2003b, MNRAS, submitted
Verner E. M., Verner D. A., Baldwin J. A., Ferland G. J., Martin P. G., 2000, ApJ, 543, 831
Viegas S., Clegg R. E. S., 1994, MNRAS, 271, 993
Walborn N. R., Blades J. C., 1997, ApJS, 112, 457 (WB97)
Walborn N. R., Fitzpatrick E. L., 1990, PASP, 102, 379
Walsh J. R., 1993, ST-ECF Newsletter, 19, 6
Walsh J. R., Rosa M. R., 1999, in Walsh J. R., Rosa M. R., eds, Proc. ESO Workshop on Chemical Evolution from Zero to High Redshift. Springer-Verlag, Berlin, p. 68
Walter D. K., Dufour R. J., Hester J. J., 1992, ApJ, 397, 196

This paper has been typeset from a TEX/LATEX file prepared by the author.